---

# Model Calibration with Variable Speed Limits on Motorways

---

*Author:*
Vasiliki KALLIGA

*Supervisor:*
Prof. Markos PAPAGEORGIOU

*A thesis submitted in fulfillment of the requirements*
*for the degree of Production Engineering and Management*

*in the*

September, 2017

"The major cause of congestion is the inefficient operation of highways during periods of high demand. "

C. Chen, Z. Jia and P.Varaiya

Technical University of Crete

# *Abstract*

Dynamic Systems and Simulation Laboratory
School of Production Engineering and Management

Diploma Thesis

**Model Calibration with Variable Speed Limits on Motorways**

by Vasiliki KALLIGA

The continuously increasing daily traffic congestions on motorway networks around the world call for innovative control measures that would drastically improve the current traffic conditions, such as the implementation of variable speed limits (VSLs). Macroscopic traffic flow models are widely used for the representation of traffic conditions. For the purposes of this study a part of the M1 motorway, in Melbourne, Australia, was calibrated with the use of the second-order, macroscopic model, METANET. The model was calibrated in CALISTO software tool, which has been appropriately extended in order to handle VSLs. Speed and flow measurements, collected from the field, are used in order to tune the simulation parameters with the purpose of replicating realistic traffic conditions. The optimization algorithm that has been applied to solve the parameter estimation problem is Nelder-Mead. The optimum set was used to validate two different days, for which we had available data. The results show a satisfactory representation of the real traffic conditions.

# *Acknowledgements*

First and foremost I would like to thank my advisor, Professor Markos Papageorgiou for his motivation, immense knowledge and for trusting me to become a member of the Dynamic Systems and Simulation Laboratory. I would like to thank Professor Ioannis Papamichail for his patience and his valuable knowledge and guidance during my first steps in the laboratory. I would also like to thank Professor Ioannis Nikolos for accepting to be a member of this thesis committee. Furthermore I am thankful to VicRoads for providing the data used.

In addition I would like to thank my friends Marianthi, Maria and Athanasia for supporting me all these years. A big thank to my parents, Ioannis and Konstantina, for everything they offered to me, as well as to my younger brother Theofanis for supporting me and giving me advices in every difficulty. I am also thankful to my dear Iordanou Konstantinos for inspiring me to do every next step of my life.

# Contents

# List of Figures

# List of Tables

*Dedicated to my family . . .*

# Chapter 1

# Introduction

Originally motorways were designed with the aim of providing unlimited mobility to the users. The continuous increase of car ownership and demand has led to the daily appearance of motorway congestion. The extent of congestion is staidly increasing in space and time. Traffic congestion reduces the available infrastructure and as a consequence the expensive motorway infrastructure is underutilized, exactly at the time that is most needed (peak hour) [1]. The consequences are huge for the economy as well as for social life. In the USA, for example, the costs related to congestion in urban areas in 2009 reached 115 billion [2].

The worst case of congestion forming is on motorways links because it affects the nominal motorway capacity and throughput due to two independent effects [3]:

- capacity drop at the head of forming congestion; and

- blocking of off-ramps by the spreading congestion body.

Both of the above impacts aggravate the infrastructure degradation. Sometimes the congestion covers a significant part of the motorway network, often spilling over from one motorway to the other via the corresponding interconnections. Daily congestion is illustrated in most metropolitan motorway networks. It should be noted that the arriving demand is typically much lower than the nominal infrastructure capacity; nevertheless the degradated infrastructure cannot serve the demand. For that reason, congestion insists until the demand falls to sufficiently low values (far below the infrastructure's nominal capacity) at the end of the peak hour. The consequences of the infrastructure degradation are more emphatic in the case of roads such as ring-roads.

It is obvious that daily congestion on motorways cannot be connected only to the excessive demand exceeding the nominal network capacity. Demand may indeed exceed temporarily and locally the motorway capacity, thus triggering local congestion; but the generalized congestion is the result of an unstable escalation caused by the degradation of the expensive infrastructure in absence of suitable traffic control measures that would counter and limit this devastating evolution.

The profitable, risk-less and less-polluting transportation of persons and goods on motorway requires an optimal utilization of the available infrastructure via suitable application of a variety of traffic measures such as variable speed limits (VSLs).

The positive impact of VSLs on traffic safety is due to the reduction and homogenization of speed that are correlated with a reduction of accident probability. Multi-year evaluations of the VSL impact on traffic safety indicate a reduction in accident numbers by as much as 20 to 30 percent after VSL installation. VSLs are also responsible for noise reduction, according to some authorities.

Some of the VSL algorithms that have been proposed and partly implemented in order to alleviate traffic congestion are known to face some limitations. VSLs are valuable for providing traffic safety, which leads to reduction of accidents, but their current usage has hardly any positive impact for the increase of throughput or for the degradation of average travel times as they are operated on the basis of very simple control strategies that cannot improve traffic flow efficiency [4] ; in addition, the range of the variable speed limits is usually limited [5].

## 1.1   Traffic Flow Models

During the last decades, a lot of mathematical models have been proposed, in order to describe the traffic flow situation on these motorways [6]. These mathematical models, can be utilized for the planning of new road infrastructures, or for the gradual change of the existing ones, with the purpose of solving the traffic jam problem. Another important use of these mathematical models is for the development and testing of traffic flow estimation algorithms, traffic control strategies and other operational tools [1].

Mathematical models consist of a set of parameters with unknown values, witch may differ in distinct networks. In case of real applications they must be properly specified, in order to reproduce the network and traffic flow condition as precise as it is possible. With respect to the details they approach the motorway they can be classify as macroscopic or microscopic. The parameters in macroscopic traffic flow models are less than in microscopic models. Also, macroscopic models have an analytical form, which allows their usage for a big variety of considerable traffic engineering tasks (estimation, control strategy design) beyond simulation. The macroscopic traffic flow models are classified as first, second or higher-order models, depending on the number of differential equations they include. First-order models are widely known for their simplicity and computational efficiency and this is the reason why they have been used extensively in the past. Nevertheless, they don't take consideration of factors such as the driver's reaction time as well as the vehicles acceleration capabilities. In addition, they are unable to capture real traffic phenomena such as capacity drop and the stop-and-go waves. On the other hand, second or higher-order models include extra equations to describe the dynamics of speed. This makes them able to reproduce the traffic phenomena mentioned above. The disadvantage in this case is the higher complexity of the models, the higher number of parameters they use and as a result the higher computational effort, which makes their use difficult in optimization problems build upon them.

## 1.2 Thesis Objectives

Given the ability of second-order models, to reproduce a lot of traffic phenomena such the ones mentioned before, this thesis examines the formulation of a popular second-order model, namely METANET [7] model. The model is applied in a real traffic network in Australia using real traffic data. The model is calibrated for this particular network, i.e the optimal parameters values are estimated using real traffic data. The calibration of the model is performed using the innovative software tool CALISTO [8] which has been recently developed and makes the calibration of traffic flow models an easy task. CALISTO has been appropriately extended for the purposes of this thesis in order to handle Variable Speed Limits (VSLs) , that are operational along the motorway considered.

## 1.3 Thesis Outline

This diploma thesis is composed of 5 Chapters. Chapter 2 presents briefly the traffic flow models and the unknown parameters that they include as well as the procedure that should be followed in order to define their values. An overview of existing VSL strategies is also presented and some background issues related to VSLs are addressed. In the same chapter, VSLs are incorporated in a second-order traffic flow model. At the beginning of Chapter 3, the model calibration procedure is presented, then the appropriately extended software tool CALISTO is described, followed by the description of the optimization algorithm Nelder-Mead [9] , which is utilized in order to solve the parameter estimation problem. Chapter 4 consist of a detailed representation of the test site network, the available data from the field and the real traffic conditions appearing on certain days. Subsequently, the calibration setup and results are presented. Finally, Chapter 5 summarizes the conclusions and presents some recommendations and potential items for future research.

# Chapter 2

# Backround

Chapter 2 presents the macroscopic traffic flow model that is used in this thesis. Section 2.1 includes a brief introduction on the traffic flow models and their classification. Furthermore, in section 2.2, the impact of Variable Speed Limits on motorways as well as on the Fundamental Diagram is presented and, finally, in Section 2.3 the METANET model is discussed.

## 2.1  Classification of Traffic Flow Models

During the last decades a great number of traffic flow models have been developed and utilized for a high variety of different traffic engineering tasks. Traffic flow models can be classified with respect to the level of detail with which the vehicular flow is described. More specifically, there are three main classes :

1. **Microscopic models** (high level of detail)

2. **Mesoscopic models** (medium level of detail)

3. **Macroscopic models** (low level of detail)

**Microscopic models** represent the space-time behavior of individual vehicles and their interactions with the surrounding traffic conditions. This behavior is described by dynamic variables such as, position, speed and acceleration. Microscopic traffic flow models require high computational effort but they provide mathematically exact simulation of the traffic flow.

**Mesoscopic models** represent the traffic flow at a lower level of detail than the previous mentioned models. Particularly, the models do not distinguish or trace the individual behavior of vehicles but they represent the behavior of small traffic groups, the activities and interactions of which are described at a medium detail level.

**Macroscopic models** represent traffic in an aggregate manner considering traffic flow as a compressible fluid with specific characteristics. The traffic variables used to describe the dynamics of this fluid are the mean speed, the density and the traffic flow (or volume). The macroscopic traffic flow models are classified as first-, second- or higher-order models, depending on the number of differential equations

they include. In this thesis a second-order model namely, METANET, is utilized using real traffic data from a freeway in Melbourne, Australia. The employed model is described in the following sections.

## 2.2   Variable Speed Limits

### 2.2.1   Existing VSL Strategies

The earliest applications of VSLs dates from the 1960s. Today, numerous applications of VSLs are encountered in many European countries, in North America and elsewhere, while their number is increasing at an accelerated pace. VSLs are applied along motorway stretches, and the speed limits are changed appropriately according to current traffic or weather conditions. The speed limits are displayed on VMSs on overhead gantries or on roadside poles, typically spaced 0.5-2 km, with sign location and visibility being an important issue for a successful system deployment. VSLs systems may operate as a standalone system or as a part of a larger system, such as an incident management system or a congestion management system.

The first step that most of the reported VSL systems follow is data collection and processing. Data are collected by means of detectors or sensors of different types, and differ depending on each application. Traffic detectors are typically used for measuring speed, flow, and occupancy. In several applications weather conditions are used as inputs, the may also benefit from surface measurements, i.e., measurements of the pavement conditions (dry, wet, salted, snowy).

The second step is the control algorithm or decision logic. The control logic is the core of VSL system operation. These systems have simple threshold-based control logics and very often the adopted thresholds are sensitive to day-to-day stochastic variations, rendering the appropriate tuning of the parameters a difficult task. Also, most of the strategies were designed without the proper knowledge on how traffic is affected by VSLs, and how the strategy should operate to accomplish a given objective.

In the third and final step the VSLs are displayed. Displays are usually updated every one or two minutes, with some systems having the update period as large as six minutes. In some applications, not only the recommended speed limit is displayed, but also a minimum speed limit. The provision of real time information such as warning messages, advices or clarification about the reasons of the system operation on additional auxiliary signs or VMSs are sometimes available, and seem to improve operation and the perception of the users about the system. In most cases, VSLs are mandatory, i.e., legally equivalent to fixed speed limits, and may even be automatically enforced to increase driver compliance and hence impact.

The list of VSL's objectives is long and extending, but could be summarized as enhanced safety, efficient motorway operation and reduction of environmental impact. More analytically:

1. **Safety**: The aim of most operational systems is to provide safety and they display safe speed limits for different road and infrastructure conditions. In these cases specific objectives are, for example, increased driver compliance and reduction of infractions, reduction of driver error (e.g., because of speeding), hazard, queue warning and consequent reduction of rear-end collision (e.g., because of an accident or congestion or fog). The stabilization of traffic flow and more uniform speeds along a lane and on different lanes are correlated with the reduction of overtaking manoeuvres and of crashes, and are, therefore, often targeted.

2. **Efficient motorway operation**: In this case the aim of the VSL systems is an efficient use of motorway facilities. Preferably, these systems target to decrease the total travel time by stabilizing the traffic flow due to more uniform speeds. Nevertheless, the results show that not too many applications achieve an improvement in traffic flow efficiency, and whenever this happened only a small improvement was obtained.

3. **Reduction of environmental impact**: As it concerns the environmental impact, not so many systems take care of this aspect. It should be noted that insignificant reductions have been reported in a few circumstances, see, e.g., [10] , [11] , [12] .

The results achieved by existing VSL operations are mixed. Several applications report up to 20-30% reduction in accident rates while others had a slight reduction in the number of accidents. It is also mentioned a reduction in average speed, better distribution of lane use and less lane change. Improvements in throughput level and reduction of travel times were most of the times minor.

### 2.2.2 The Fundamental Diagram

Under the assumption that traffic conditions do not change in space and time the traffic flow states may be approximated by the so-called fundamental diagram (FD), which may be a speed-flow diagram or a flow-occupancy diagram (see figure 2.1). It should be mentioned that the mean speed of a particular traffic state on the diagram is proportional to the slope of the line that connects the particular traffic state point with the origin. A fundamental diagram may be obtained by collecting measurements of the related traffic variables (flow and occupancy or mean speed) , at a specific motorway stretch and fitting the appropriate mathematical function (see [4] for more details) .
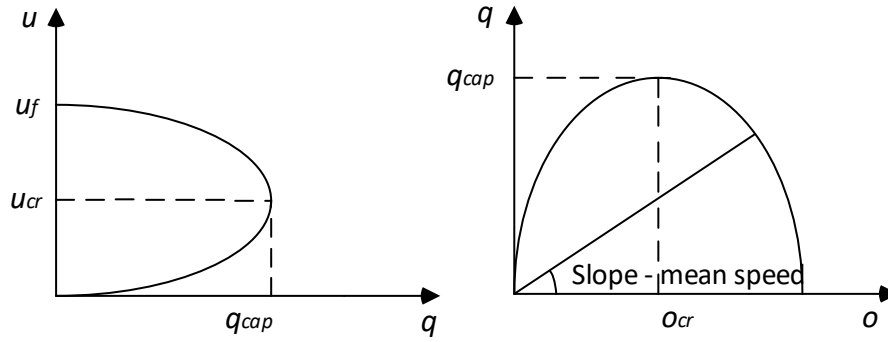
FIGURE 2.1: Speed-flow diagram (left) and flow-occupancy diagram (right) where: $u$ is the mean speed (km/h), $u_f$ is the free speed(km/h) and $u_{cr}$ is the critical mean speed (km/h). Flow-occupancy diagram (right): $q$ is the flow (veh/h), $q_{cap}$ is the capacity flow(veh/h), $o$ is the occupancy (%), $o_{cr}$ is critical occupancy (per cent)

### 2.2.3 The Impact of VSLs on the Fundamental Diagram

As mentioned earlier, there were very few investigations in the past addressing the impact of VSLs on aggregate traffic flow behavior, e.g., on the fundamental diagram. Some early investigations based on a two-lane motorway in Germany indicated a speed homogenization effect (less speed differences) for vehicles [13] . These results are really useful for a better understanding of the VSL impact on individual vehicles. Figure 2.2 (a) illustrates that *"at lower or mean traffic volumes, the mean speed is lower due to the reduction effect whereas, at higher volumes, an increase is detected due to the stability effect."* [14].
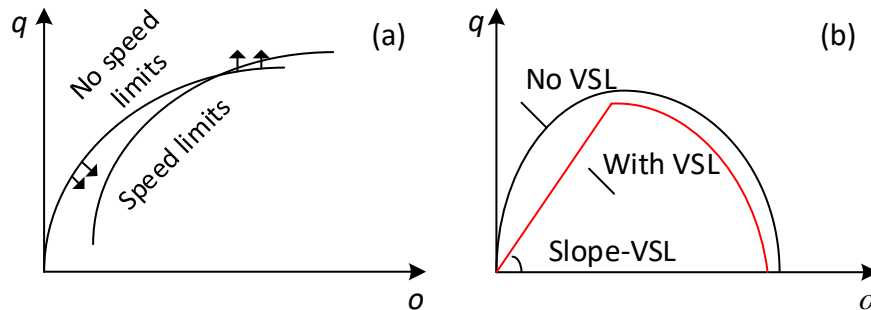


FIGURE 2.2: (a) Change of the fundamental diagram because of speed limits [14]; (b) Hegyi model for VSL impact [15]

In a more recent work regarding VSL, the assumed VSL impact was to merely replace the left part of the flow-occupancy curve by a straight line with slope corresponding to the displayed VSL (see figure 2.2 (b)) [15] .

According to the Hegyi model (see Figure 2.2 (b)), both flow-density curves (for VSL and non-VSL) meet but not actually cross while Zackor [14] suggests that there is actually a valid cross-point of both curves somewhere near the critical occupancy (Figure 2.2 (a)). The cross-points (if any) are likely to lie at increasing occupancy values for decreasing VSLs because of the accordingly decreasing slope of the under-critical VSL-affected curves. In fact, there may be no cross-point for very low VSLs.

### 2.2.4 VSL's Influence at Mean Speed

It seems quite reasonable to assume that a VSL displayed at under-critical occupancies will reduce (with reasonable driver compliance) the (otherwise higher) mean speed (see Figure 2.3 (a)). The extent of this effect is likely to depend on the displayed VSL as well as on driver compliance. The new VSL-affected states serve the same flow at lower speed and higher occupancy than the original states, which indicates that the travel time increases accordingly. In the case of applying VSLs at under-critical traffic states it is likely to increase travel times and consequently decline traffic flow efficiency.
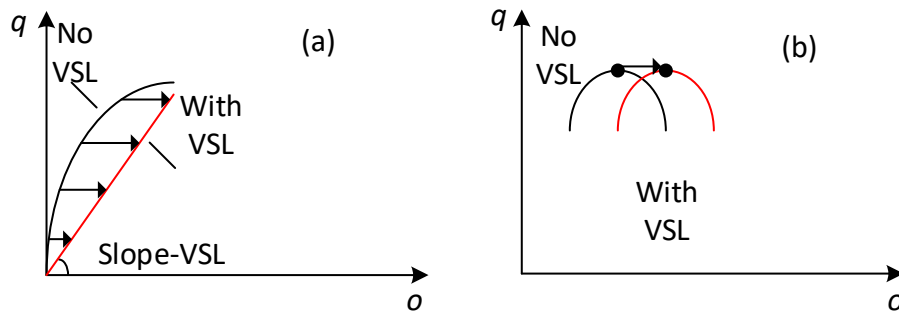


FIGURE 2.3: (a) Potential effect of VSL on under-critical occupancies; (b) cross-point of diagrams with and without VSLs

It is quite important to emphasize that if a VSL system is applied upstream of a bottleneck that is close to be active, this will decrease for a while the mainstream flow that arrives at the bottleneck area, consequently a delay in the bottleneck activation appears. It seems quite reasonable that the occupancy in the VSL situation is higher than in the non-VSL state. Note that the temporary flow decrease during the VSL-triggered traffic state transition is because of the fact that occupancy (and density) in the VSL state is higher than in the original non-VSL state; thus, during the transition the flow is temporarily reduced to "create" the higher traffic density of the VSL state. It should be noted that this is the main VSL impact exploited exploited by [15].

### 2.2.5   The Effect of VSLs on Traffic Behavior

The effect of VSLs on aggregate traffic flow behavior is significant. Some of the most important are summarized as follows [4] :

1. The application of speed limits at under-critical occupancies have the effect of decreasing the slope of the flow-occupancy diagram. In addition, the smaller imposed the the speed limit, the larger the decrease in the slope of the flow-occupancy diagram. This effect may be exploited to hold back traffic flow to retard the onset of congestion at downstream bottlenecks [15].

2. With respect to the potential increase of flow capacity, there is an inconclusive result, because a slight increase may be visible for some VSL values while at other locations no capacity increase can be observed for any VSL value [16] .

3. The VSL-affected flow-occupancy curve crosses the non-VSL curve, shifting the critical occupancy to higher values in the flow-occupancy diagram. This effect holds more vehicles in the motorway without falling into congestion.

4. Regardless of whether the flow capacity is increased for some VSLs or not, it is clear that low VSLs lead to accordingly lower flow capacity in the fundamental diagram than in non-VSL case.

## 2.3   METANET Traffic Flow Modeling

A macroscopic second-order traffic flow model is used in this thesis. The model was calibrated and validated against real traffic data and was found to reproduce the whole range of real traffic conditions (free flow, critical, congested) with acceptable accuracy.

### 2.3.1   Introductory

METANET [7] is a program for motorway network simulation based on a purely macroscopic modeling approach. It is a discretized and enhanced variation of the second order model of Payne [17]. The motorway network is represented by a directed graph whereby the links of the graph represent motorway stretches. Each motorway stretch has uniform characteristics, i.e., no on- or off-ramps and no major changes in geometry. The nodes of the graph are placed at locations where major changes in road geometry occur as well as at junctions, on-ramps, and off-ramps.

   The macroscopic description of traffic flow implies the definition of adequate variables expressing the aggregate behavior of traffic at certain times and locations. The time and space arguments are discretized. The discrete-time step is denoted by $T$. A motorway link $m$ is divided into $N_m$ segments of equal length $L_m$ (Figure 2.4). The traffic in each segment $i$ of link $m$ at discrete-time $t = k\,T$, $k = 0, 1, \ldots, K$, where $k$ is the time horizon, is macroscopically characterized via the following variables:

the traffic density $\rho_{m,i}(k)$ (veh/km/lane) is the number of vehicles in segment $i$ of link $m$ at time $t = k\,T$ divided by $L_m$ and by the number of lanes $\lambda_i$ ; the mean speed $v_{m,i}(k)$ (km/h) is the mean speed of the vehicles included in segment $i$ of link $m$ at time $t = k\,T$; and the traffic volume or flow $q_{m,i}(k)$ (veh/h) is the number of vehicles leaving segment $i$ of link $m$ during the time period $[k\,T, (k+1)T]$ divided by $T$.
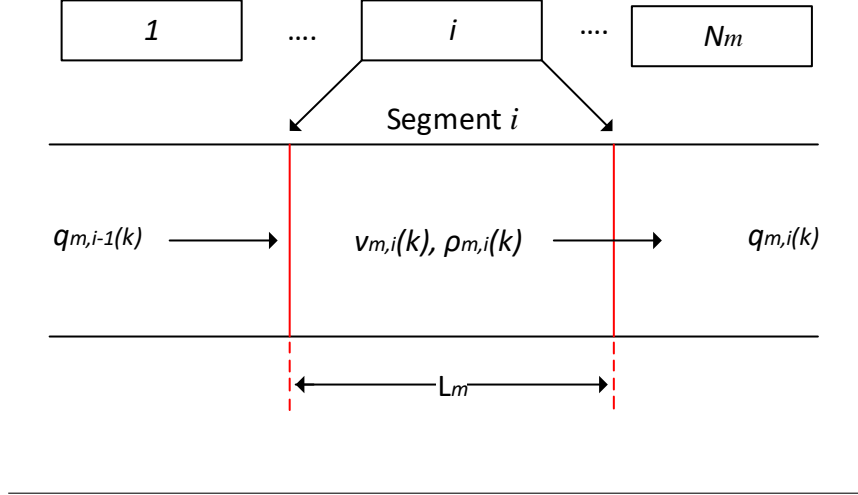


FIGURE 2.4: Discretized motorway link.

The previous defined traffic variables are calculated for each segment $i$ of link $m$ at each time step $k$ by the following equations:

$$\rho_{m,i}(k+1) = \rho_{m,i}(k) + \frac{T}{L_m \lambda_m}\big[q_{m,i-1}(k) - q_{m,i}(k)\big] \tag{2.1}$$

$$q_{m,i}(k) = v_{m,i}(k)\rho_{m,i}(k)\lambda_m \tag{2.2}$$

$$v_{m,i}(k+1) = v_{m,i}(k) + \frac{T}{L_m}v_{m,i}(k)\big[v_{m,i-1}(k) - v_{m,i}(k)\big]$$
$$+\frac{T}{\tau}\big[V(\rho_{m,i}(k) - v_{m,i}(k))\big] - \frac{\nu T}{\tau L_m}\left[\frac{\rho_{m,i-1}(k) - \rho_{m,i}(k)}{\rho_{m,i}(k) + \kappa}\right] \tag{2.3}$$

where 2.1 is the conservation equation; 2.2 is the transport equation to be replaced in 2.1; 2.3 is an empirical dynamic mean speed equation where 2.4, the static speed-density relationship corresponding to the fundamental diagram, must be replaced; and $\tau$ (a time constant), $\nu$ (an anticipation constant) and $\kappa$ are model parameters. Two further terms may be added to 2.3 for higher accuracy under certain conditions [18]. The following function corresponds to the fundamental diagram and is calculated as follows:

$$V[\rho_{m,i}(k)] = v_{f,m}exp\left[-\frac{1}{a_m}\left(\frac{\rho_{m,i}(k)}{\rho_{cr,m}}\right)^{a_m}\right] \tag{2.4}$$

where $v_{f,m}$ is the free speed, $\rho_{cr,i}$ is the critical density (for which the flow at section $i$ is maximized) and $\alpha_i$ is a further model parameter for section $i$. Furthermore, a minimum value $v_{min}$ should not be exceeded by the mean speed calculated by the model. The two additional terms, [18], were proposed for more accurate modeling of merging and lane drop phenomena. More specifically, the impact on mainstream speed due to an on-ramp merging flow is considered by adding the term $\left[-\delta T q_\mu(k)v_i(k)/\left(L_i\,\lambda_i[\rho_i(k)+\kappa]\right)\right]$ at the right hand-side of 2.3 for all the merging section, where $\delta$ is a model parameter and $q_\mu$ is the inflow from the on-ramp. In order to take into-account the impact to speed due to intensive lane-changing at lane-drop areas, the term $\left[-\phi T\Delta\lambda\rho_i(k)v_i(k)^2/\left(L_i\lambda_i\,\rho_{cr,i}\right)\right]$, is added to 2.3 for the section immediately upstream of the drop, where $\phi$ is a model parameter and $\Delta\lambda$ is the number of dropped lanes.

The original (non-VSL) model includes the following three constant parameters in the speed-density curve: the free speed $v_{f,m}$ encountered at zero density ($\rho_{m,i}{=}0$), the critical density $\rho_{cr,m}$ at which traffic flow is close to capacity $q_{cap,m}$ and $\alpha_m$. Combining 2.2-2.4 under stationary conditions (i.e., $v_{m,i}(k{+}1){=}v_{m,i}(k)$) and spacially homogeneous conditions (i.e., $u_{m,i-1}{=}v_{m,i}$ and $\rho_{m,i+1}{=}\rho_{m,i}$) yields the capacity of the fundamental diagram (flow-density curve) :

$$q_{cap,m} = v_{f,m}\rho_{cr,m}exp\left[-\frac{1}{\alpha_m}\right] \tag{2.5}$$

METANET may be applied to existing or hypothetical, multi-origin, multi destination, multi-route motorway networks with various topology and geometric characteristics including bifurcations, junctions, on-ramps and off-ramps. In general link bounds are represented by nodes. Traffic enters a node $n$ through a number of input links according to the following equations:

$$Q_n(k) = \sum_{\mu\in I_n} q_{\mu,N_\mu}(k) \tag{2.6}$$

$$q_{m,0} = \beta_n{}^{\mathrm{m}}(k)Q_n(k) \quad \forall m \in O_n \tag{2.7}$$

$I_n$ is the set of links entering node $n$, $O_n$ is the set of links leaving $n$, $Q_n(k)$ is the total traffic volume entering $n$ at period $k$, $q_{m,0}(k)$ is the traffic volume that leaves $n$ via out-link $m$, and $\beta_n{}^{\mathrm{m}} \in [0,1]$ is the portion of $Q_n(k)$ that leaves $n$ through link $m$ (turning rates).

At a network node $n$, the upstream influence of the downstream link density (e.g., is case of congestion spill-back) has to be taken into account in the last segment of the incoming links. This is provided via

$$\rho_{m,N_m+1}(k) = \frac{\sum_{\mu\in O_n} \rho_{\mu,1}^2(k)}{\sum_{\mu\in O_n} \rho_{\mu,1}(k)} \tag{2.8}$$

where $\rho_{m,N_m+1}(k)$ is the virtual density downstream of any entering link $m$ to be used in 2.3 for $i = N_m$ and $\rho_{\mu,1}(k)$ is the density of the first segment of the leaving

link $\mu$. The quadratic form is used to account for the fact that congestion on one leaving link may spill back into the entering link even if there is free flow in the other leaving links.

Similarly, at a network node $n$, the downstream influence of the upstream-link speed has to be taken into account according to 2.3 for $i = 1$. The required mean speed value is calculated from the flow-weighted average

$$u_{m,0}(k) = \frac{\sum_{\mu \in I_n} u_{\mu,N_\mu}(k) q_{\mu,N_\mu}(k)}{\sum_{\mu \in I_n} q_{\mu,N_\mu}(k)} \tag{2.9}$$

where $u_{m,0}(k)$ is the virtual speed upstream of any leaving link $m$ that is neede in 2.3 for $i = 1$.

### 2.3.2  Incorporating the VSL Impact

The described model may be extended to incorporate the impact of displayed VSL values on the traffic flow behavior under the assumption that a single VSL value (if any) is displayed in each link (using, in real implementations, as many gantries as necessary, depending on the link length) . It should be noted that this assumption is not really restrictive because if a higher spatial granularity of VSL values is desired, links may be selected accordingly short. Contrary, if a lower spatial granularity of VSL values $i$ desired, there is a possibility for the user of the related software tool METANET to create clusters of links, each cluster having a common VSL value.

It should be specified that, particular VSL values are reflected in the link-specific VSL rates $b(k)$ that prevail during $[kT, (k+1)T]$. VSL rates are naturally control variables with an admissible value range $b(k) \in$ (0,1).

Using the defined VSL rates, the static speed-density relationship 2.4 becomes b-dependent [19]. This is enabled by actually rendering the three parameters included in 2.4 b-depended by use of the following linear functions:

$$v_f^*[b(k)] = v_f b(k) \tag{2.10}$$

$$\rho_{cr}^*[b(k)] = \rho_{cr}\{1 + A[1 - b(k)]\} \tag{2.11}$$

$$\alpha^*[b(k)] = a\big[E - (E - 1)b(k)\big] \tag{2.12}$$

where $v_f$, $\rho_{cr}$ and $\alpha$ denote the specific non-VSL values for these parameters in 2.4, while $A$ and $E$ are constant parameters to be estimated based on real data.

As 2.10 reveals, $b$ is equal to the VSL-induced $v_f^*$ divided by the non-VSL $v_f$ or approximately equal to the displayed VSL divided by the legal speed limit without VSL. Hence, if $b(k)$=1, no VSL is applied, else $b(k) < 1$, all parameters are seen in 2.10 - 2.12 to attain their respective non-VSL values. Equations 2.11 and 2.12 suggest

that for $A > 0$ and $E > 1$, $\rho_{cr}^*$ and $a^*$ are similar increasing functions for decreasing $b$ starting with their usual non-VSL values for $b(k){=}1$.

For the extended model, 2.4 in then replaced by :

$$V[\rho_{m,i}(k), b_m(k)] = v_{f,m}^*[b_m(k)]exp\left[ -\frac{1}{a_m^*[b_m(k)]}\left(\frac{\rho_{m,i}(k)}{\rho_{cr,m}^*[b_m(k)]}\right)^{a^*[b_m(k)]}\right] \quad (2.13)$$

and $V(\rho_{m,i}(k))$ in 2.3 now reads $V(\rho_{m,i}(k),b_m(k)$ while VSL-induced capacity flow is give by :

$$q_{cap}^*[b(k)] = u_f^*[b(k)]\rho_{cr}^*[b(k)]exp\left( -\frac{1}{a^*[b(k)]}\right) \quad (2.14)$$

The model was calibrated by use of traffic data taken from an Australian VSL-equipped motorway location, where the legal speed limit is 100 km/h and the applied VSL values are 80 km/h and 60 km/h. (These values corresponds to VSL rates $b \in \{1,0.8,0.6\}$ see Figures B.1- B.3). The results of the calibration are presented in Chapter 4.

# Chapter 3

# Traffic Flow Model Calibration

Chapter 3 briefly presents the procedure in order to specify the unknown model parameter values for a particular freeway site. More specifically, Section 3.1 describes the model calibration procedure, Section 3.2 presents the software tool that will be employed to calibrate the investigated traffic flow model and Section 3.3 presents the optimization algorithm that will solve the parameter estimation problem.

## 3.1  Model Calibration Procedure

The aim of the model parameter estimation, or parameter calibration, procedure is to enable a macroscopic traffic flow model to represent traffic conditions of a motorway with the highest achievable accuracy. The estimation of the unknown model parameters is not an easy task, since the system equations are highly nonlinear in both the parameters and the state variables. Consider that a macroscopic discrete-time sate-space model is described by the following state equations:

$$\mathbf{x}(k+1) = f[\mathbf{x}(k), \mathbf{d}(k), \mathbf{p}] \qquad k = 0, 1, \ldots, K-1 \tag{3.1}$$

$$\mathbf{x}(0) = \mathbf{x}_0$$

where $\mathbf{x}$ stands for the state vector, $\mathbf{d}$ is the disturbance (external variable) vector and $\mathbf{p}$ is the parameter vector. The METANET model can readily assume the state-space form 3.1 for any freeway network. More specifically, the state vector $\mathbf{x}$ consist of the section densities and mean speeds, the external variable vector $\mathbf{d}$ includes the origin speeds and inflows, the turning rates at bifurcations, and the downstream densities; and finally $\mathbf{p}$ includes the unknown model parameters that need to be specified.

The optimization cycle is briefly described in Figure 3.1. Assuming that the initial state $\mathbf{x}_0$ is given, as well as the external vector $\mathbf{d}(k)$ is known over a time horizon $k=0,1,\ldots,K$-1, the parameter estimation problem can be formulated as a nonlinear least-squares output error problem which targets at the minimization of the discrepancy between the model calculations and the real traffic data by use of the following cost function,
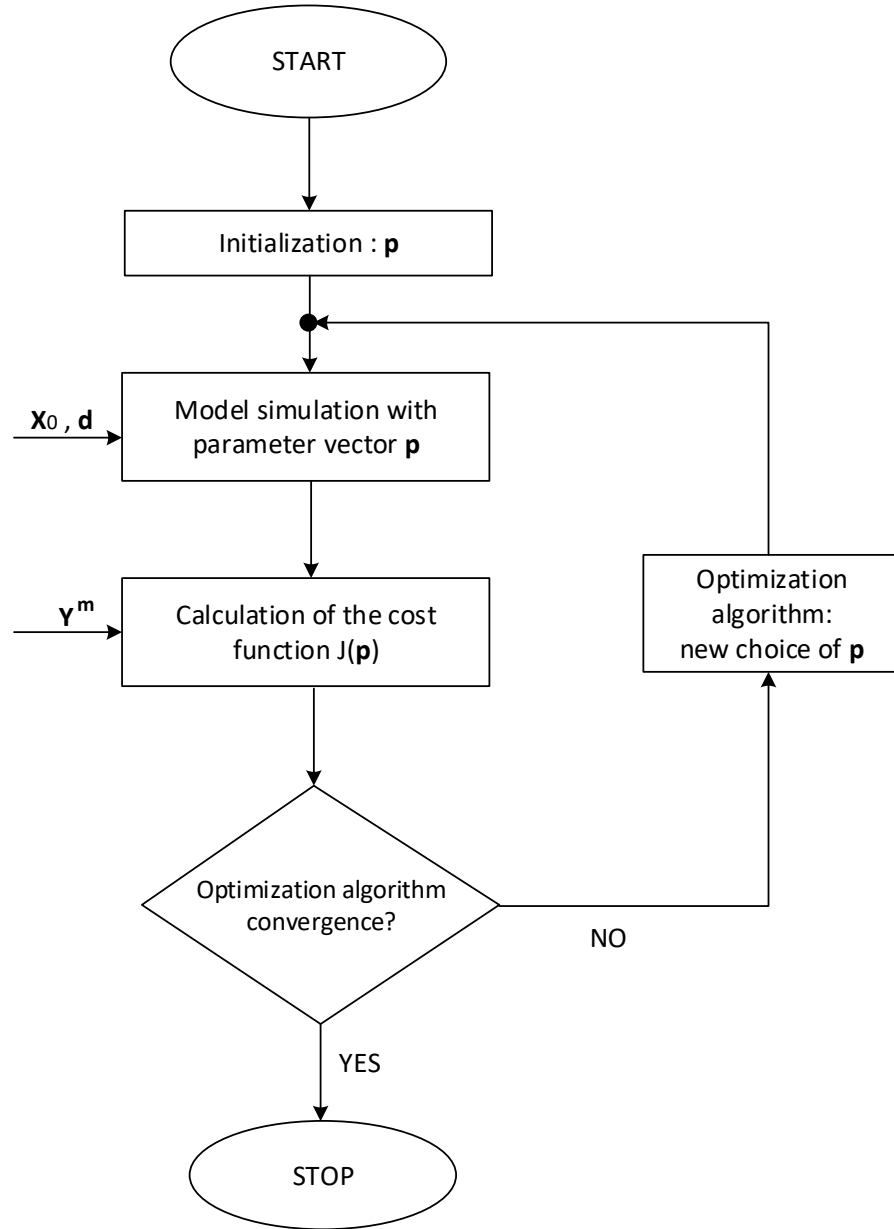
FIGURE 3.1: Model calibration procedure

$$J(\mathbf{p}) = \sqrt{\frac{1}{k} \sum_{k=0}^{K-1} [\mathbf{y}(k) - \mathbf{y^m}(k)]^2} \qquad (3.2)$$

subject to 3.1; where $\mathbf{y}\,(k)=\mathbf{g}[\mathbf{x}(k)]$ is the measurable model output vector (typically consisting of flows and mean speeds at various network locations) and $\mathbf{y}^m$ includes the real measured traffic data (consisting of flows and speeds at corresponding network locations). The model parameter values are selected from a closed admissible

region of the parameter space, which may be defined on the basis of physical considerations and previous experience. The determination of the optimal parameter set must be performed by means of a suitable nonlinear programming routine, whereby for each choice of a new parameter vector **p**, the value of the performance index (PI) of the Equation 3.2 may be computed by a calibration run of the model equations as shown in Figure 3.1. In addition, the procedure for the calculation of the cost criterion is illustrated in Figure 3.2.
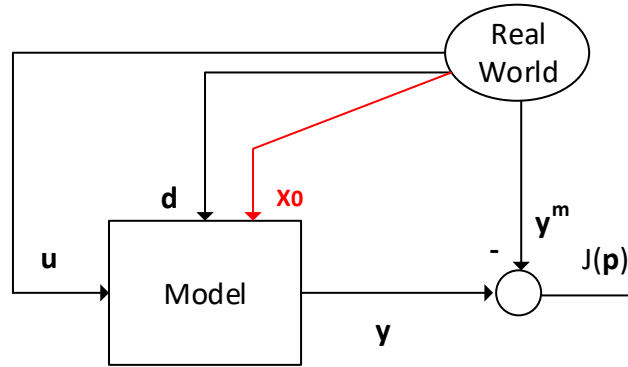


FIGURE 3.2: Calculation of Cost Criterion

Gradient-based optimization algorithms are not a solution for the case of the nonlinear, non-convex least-squares optimization problem, because it is known that they have multiple local minimum [20]. In previous calibration studies, various derivative-free optimization algorithms have been employed to solve the parameter estimation problem, without much insight regarding their respective properties for the particular problem at hand. Within this thesis, the Nelder-Mead stochastic algorithm is tested for the problem of macroscopic traffic flow model calibration.

## 3.2 CALISTO Software Tool

The previously developed CALISTO ( CALIbration Tool) [8] is a software tool which enables the calibration and validation of macroscopic traffic flow models for various freeway sites using real traffic data. For the purposes of this study, CALISTO was appropriately extended in order to handle VSLs. More specifically, the METANET model's functions with the VSL's impact, as described in Chapter 2, were incorporated. This section briefly describes the software.

### 3.2.1   CALISTO Input Data

In order to find the optimum values of the unknown model parameters CALISTO requires some basic elements. To begin with, *Freeway Network Description* is the first input that CALISTO ask for. An editor is opened which includes all the required information needed so that a freeway site is described sufficiently, such as the number of freeway links, the number of freeway on-ramps and off-ramps, the number of detector stations, and after the last extension of this software tool, the user can insert information about the variable speeds limits (VSLs) that exist in the freeway stretch.

Moreover, *Simulated traffic data* is an input that is also required. It contains information about the simulation data, such as the simulation step, the traffic measurements interval, the simulation duration etc., as well as the specification of the traffic input data.

Some *Other settings* are also necessary. They consist of some extra simulation features and the flow and speed error weights included in the calculation of the performance index. In particular, the utilized performance index (within the software) is given by the following equation:

$$PI = w_f \times RMSE_{flows} + w_s \times RMSE_{speeds} \tag{3.3}$$

where $RMSE_{flows}$ and $RMSE_{speeds}$ are the root mean squared errors of the real flow and speed measurements and the corresponding model estimations, respectively, and $w_f$ and $w_s$ are the corresponding error weights. For the purposes of this thesis $w_s$=1 and $w_f$=0. The editor also includes some choices regarding the simulation output plots.

Furthermore, the *Selection of traffic flow model* is needed. In this step one of the available traffic flow models can be selected and the corresponding model parameter values should be specified. In the current version of the software there are two available macroscopic traffic flow models; namely, the first-order model CTM [21] and the second-order model METANET [7]. For the purposes of this thesis only the second-order model METANET will be utilized.

In addition, the *Selection of optimization algorithm* should be specified. One of the available optimization methods can be employed to perform the calibration of the chosen traffic flow model, using particular algorithm parameters. In the current version of the software there are three available optimization algorithms. For the purpose of this study the deterministic Nelder-Mead algorithm is utilized.

The next step consist of the *Selection of the operation*. There are two choices, either *Calibration* or *Validation*. The calibration aims at the estimation of the optimal model parameter values so that the model may represent the traffic conditions of a particular freeway site with the highest achievable accuracy. The validation, is usually carried out after the model calibration, and aims to test the validity of the produced model, thus the resulting model is applied to the same freeway site using different traffic data than the data used for its calibration.

The final step is the *Execution*, where the selected operation is executed taking into account all the introduced information.

### 3.2.2 Traffic Flow Model Selection

As already mentioned, two traffic flow models are available in the current version of the software. Both models are discrete-time state-space models and they are the most commonly used models for the freeway traffic flow representation.

For the purposes of this study the second-order model METANET was selected. In this case the global parameters to be defined are the following :

- $\tau$ : a time parameter in sec.

- $\nu$: an anticipation parameter in $km^2/h$

- $\delta$ : a merging parameter in h/km

- $\phi$ : a lane-drop parameter in h/km

- $\kappa$ : a further model parameter in veh/km/lane

- $v_{min}$ : the minimum speed in km/h.

Moreover, it should be indicated, for each one of the above parameters, whether it should be considered as fixed, by selecting one of the options of the list box located next to each parameter. If a parameter is defined as fixed, it will not be taken into account in the calibration procedure, and the assigned value will considered instead.

Furthermore, every freeway link should be assigned to one of the listed FD groups, by ticking on the corresponding Link-Group combination. Finally, the definition of the parameters for each group should be specified. In particular the parameters that need to be specified are:

- $v_f$ : the free flow speed in km/h.

- $\rho_{cr}$ : the critical density in veh/km/lane

- $\alpha$ : a further parameter.

Note that, CALISTO software tool was appropriately extended in order to handle with VSLs. For this reason two more parameters are required in order to be calibrated our network. These two extra parameters are :

- $A$ : constant parameter to be estimated based on real data.

- $E$ : a further parameter to be estimated based on real data.

### 3.2.3   Optimization Algorithm Selection

As it follows, the optimization algorithm should be specified. In the current version of the software three optimization algorithms are available. Namely, the Nelder-Mead method, a genetic algorithm and the cross-entropy method [9]. All three optimization methods are derivative free methods and are suitable suitable for the calibration of macroscopic traffic flow model. In this thesis the *Nelder-Mead* is selected and the following parameters should be specified :

- Tol.fun.: Termination tolerance on the performance index value.

- Tol.x.: Termination tolerance on the parameter vector values.

- Max.iter.: Maximum number of iterations allowed.

More information about the method and its parameters are provided in Section 3.3.

### 3.2.4   Calibration/Validation Results

The delivered results depend on the selected operation. Two are the possible options:

1. **Calibration**: In this case a graph of the calibration progress over iterations is illustrated. This graph appears only if this is selected by the user. Also, a window appears which includes a set of the optimum values for the model parameters. In addition, time plots are illustrated of the real traffic measurements (flows, speeds, densities) and the corresponding model estimations for all detector locations. These plots appear only if selected by the user. Finally, some output files are produced, including all the information related to the calibration results (e.g. optimal parameter values, flow, speed and density estimations at all network segments, performance index value, etc.)

2. **Validation**: If the selected operation is Validation, then some time plots of the real traffic measurements (flows, speeds and densities) are obtained to the results, and the corresponding model estimations for all detector locations. Furthermore, the output files are produced, which include all the information related to the validation results (e.g flow, speed and density estimations at all network segments, performance index value, etc.)

In the following Chapter the extended CALISTO software will be utilized to calibrate the METANET model, using real traffic data from the M1 motorway in Melbourne, Australia, and by employing one of the available optimization algorithms.

## 3.3 Nonlinear Programming Methods

There are several optimization algorithms to solve the parameter estimation problem; since the investigated objective function has many local minima. The application of algorithms which do not use gradients is required [9]. The nonlinear programming methods, that are suitable are mainly heuristic algorithms which combine local search procedures and higher level strategies, creating this way a process which is capable to avoid bad local minima.

More specifically, the algorithms that could be used in order to solve the parameter estimation problem are :

1. **The deterministic Nelder-Mead method**

2. **The stochastic Cross-Entropy Method**

3. **The Genetic Algorithms**

4. **The Simulated Annealing Optimization**

5. **The Particle-Swarm Optimization**

### 3.3.1 Nelder-Mead Algorithm

For the purposes of this thesis the Nelder-Mead algorithm (Nelder and Mead, 1965) is employed to solve the model parameter estimation problem. Nelder-Mead is one of the best known algorithms for multidimensional optimization [9]. The method does not require any derivative information which makes it suitable for problems with non-linear, discontinuous or stochastic cost function. It has been designed to solve classical optimization problems without constraints in order to minimize a given nonlinear function $f{:}R^n \to R$. It is a direct method since it uses only some function evaluations at some points of $R^n$.

The method uses a simplex, as shown in Figure 3.3, i.e. a n-dimensional shape with $n+1$ vertices [22]. Every vertex $\mathbf{p}_i$, where $i$=1,2,...,$n$+1, corresponds to a potential solution which in turn corresponds to a cost function value, $\mathbf{J}(\mathbf{p}_i)$. The algorithm starts with an initial working simplex and then performs a sequence of transformations aiming at reducing the cost function value at its vertices.

More specifically, each iteration of the Nelder-Mead algorithm consist of the following steps.

- **Ordering:** The algorithm orders the simplex vertices with respect to the corresponding cost function values to satisfy $\mathbf{J}(\mathbf{p}_1) \leq \mathbf{J}(\mathbf{p}_2) \leq \ldots \leq \mathbf{J}(\mathbf{p}_{n+1})$ .

- **Centroid:** The algorithm calculates the centroid $\mathbf{p}_c$ of all vertices excluding the worst vertex $\mathbf{p}_{n+1}$
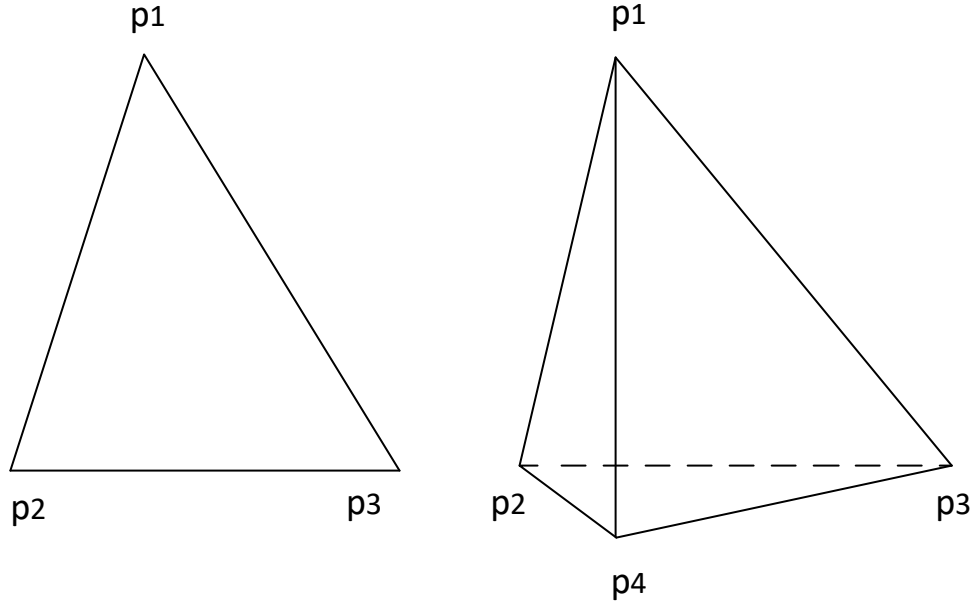
p1

p2                    p3      p2                    p3

p4

FIGURE 3.3: Example of a Simplex in $R_2$ (triangle), and a Simplex in $R_3$(tetrahendron)

- **Transformation:** The new working simplex is computed from the current one as follows. Firstly, an attempt is made to replace only the worst vertex $\mathbf{p}_{n+1}$ with a better point by using *reflection*, *expansion* or *contraction*. In the case that this succeeds, then the accepted point becomes the new vertex of the working simplex.In the opposite case, if this falls, the algorithm shrinks the simplex towards the best vertex $\mathbf{p}_1$. In this case, $n$ new vertices are computed.

In the following, a detailed description of the working simplex transformations is presented:

1. **Reflection:** The algorithm computes the reflected point $\mathbf{p}_r = \mathbf{p}_c + \zeta(\mathbf{p}_c - \mathbf{p}_{n+1})$. If the reflected point is better than the second worst, but not better than the best i.e: $\mathbf{J}(\mathbf{p}_1)<\mathbf{J}(\mathbf{p}_r)<\mathbf{J}(\mathbf{p}_n)$ then the worst point $\mathbf{p}_{n+1}$ is replaced with the aim of the new working simplex by the reflection point $\mathbf{p}_r$ and the algorithm returns the first step.

2. **Expansion:** If the reflected point is the best point computed so far, i.e: $\mathbf{J}(\mathbf{p}_r)<\mathbf{J}(\mathbf{p}_1)$, then the method computes the expanded point $\mathbf{p}_e=\mathbf{p}_c+x(\mathbf{p}_c-\mathbf{p}_{n+1})$. In the opposite case, if the reflected point is worse than the expanded point, $\mathbf{J}(\mathbf{p}_e)<\mathbf{J}(\mathbf{p}_r)$, then the worst point $\mathbf{p}_{n+1}$ is replaced with the aim of the new working place by the expanded point $\mathbf{p}_e$ and the algorithm returns to the first point. Otherwise, the new working simplex is obtaining by replacing the worst point $\mathbf{p}_{n+1}$ with the reflected point $\mathbf{p}_r$ and the algorithm returns to the first step.

3. **Contraction:** In the case of $\mathbf{J}(\mathbf{p}_n) \leq \mathbf{J}(\mathbf{p}_r)$, the *contraction* point $\mathbf{p}_{contr}$ is computed as $\mathbf{p}_{contr}=\mathbf{p}_c+\gamma(\mathbf{p}_c\text{-}\mathbf{p}_{n+1})$. Furthermore, if $\mathbf{J}(\mathbf{p}_{contr})<\mathbf{J}(\mathbf{p}_{n+1})$ then the worst point $\mathbf{p}_{n+1}$ is replaced with the aim of the new working simplex by the *contracted* point $\mathbf{p}_{contr}$ and the algorithm returns to the first step. Otherwise, the algorithm performs a shrink transformation.

4. **Shrink:** The algorithm replaces all points, except for the best, using the equation $\mathbf{p}_i=\mathbf{p}_1+\sigma(\mathbf{p}_i\text{-}\mathbf{p}_1)$ for all $i \in [2,\ldots,n+1]$

The simplex transformations in the Nelder-Mead are controlled by four parameters:

1. $\zeta$ for *reflection*. A typical value for this parameter is $\zeta$=1.

2. $\chi$ for *contraction*. A typical value for this parameter is $\chi$=1.

3. $\gamma$ for *expansion*. A typical value for this parameter is $\gamma$=2.

4. $\sigma$ for *shrinkage*. A typical value for this parameter is $\sigma=\frac{1}{2}$.

The procedure described above continues until the working simplex becomes sufficiently small or when the values $\mathbf{J}(\mathbf{p}_i)$ are close enough to each other.

### 3.3.2 Advantages and Disadvantages

The method often gives significant ameliorations of the cost function values and satisfactory results are produced quite fast. In addition, typically only one or two function evaluations per iteration are required by the Nelder-Mead algorithm. The only exception is in shrink transformations, which are not really common in practice.This is very useful in applications where each function evaluations is very time-consuming or expensive. For this kind of problems, the method is faster than other methods, especially those that require at least *n* function evaluations per iteration. In contrast, some times the method may make a huge number of iterations without significant improvement of the cost function value. A heuristic solution for this phenomenon, is to restart the algorithm several times, with reasonably small number of allowed iterations per each run. In addition, the evaluation of the working simplex and the produced best solution are depended on the initial working simplex, since the algorithm searches for the new points using the vertices of the working simplex. To face this fact, multiple algorithm runs should be carried out using different vertices for the working simplex (for more details see [23]).

# Chapter 4

# Implementation

Chapter 4 includes a description of the test site network and the calibration set-up of the second-order model METANET. More specifically, Section 4.1 describes the examined freeway site and the real traffic data used in the presented investigations. Section 4.2 consist of the calibration set-up for the METANET model use of the extended tool CALISTO. Finally, Section 4.3 presents the calibration results.

## 4.1 Network Setup

### 4.1.1 Test Site and Traffic Data

The network studied in this thesis is a stretch of the motorway M1 located in Melbourne, Australia. The case study concerns the in-bound part of the freeway. The necessary input data for the macroscopic simulator and for the evaluation of the models output where delivered by VicRoads (November and August, 2016).
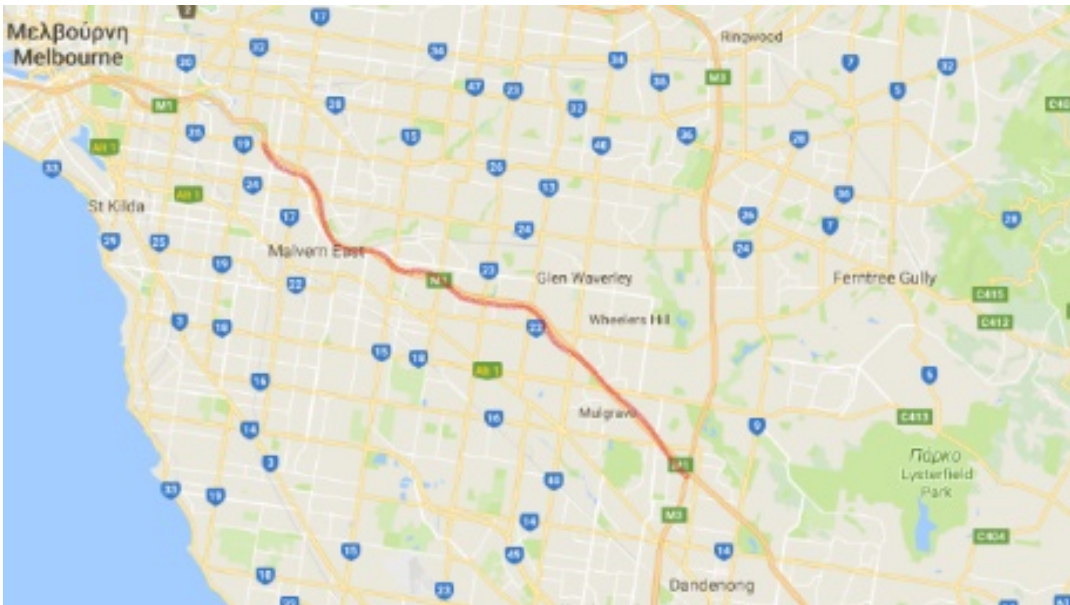


FIGURE 4.1: Test Site Network

Google Earth assisted to obtain a detailed representation of the network in the macroscopic simulator. It was used in order to define the geometric characteristics of

the freeway as well as to determine the exact location of each detector from which we have obtained the data. To reproduce, the observed traffic conditions, it is really important to use traffic data from different parts of the study network stretch. The numerous detectors placed along each lane of the freeway give us a good overview of the traffic conditions. As a consequence, the complex infrastructural features make this site an interesting case of a network to calibrate.

The available data for the test site network consist of the per minute (60 seconds) traffic flow and speed measurements from detectors placed along the examined stretch from multiply days in 2016, more specifically in the months November and August. Note that the duration of the examined measurements remains the same from day to day, in particular the morning peak hours 05.00:11.00 AM.

| Date | Period |
|---|---|
| Monday 15/8/2016 | 05.00:11.00 AM |
| Tuesday 16/82016 | 05.00:11.00 AM |
| Thursday 18/8/2016 | 05.00:11.00 AM |
| Tuesday 8/11/2016 | 05.00:11.00 AM |
| Wednesday 9/11/2016 | 05.00:11.00 AM |
| Friday 11/11/2016 | 05.00:11.00 AM |

TABLE 4.1: Available real data for the test site network

The implemented network is a stretch of 15.86 km in length ($25^{th}$ to $10^{th}$ km, direction to the city) and it is composed by four lanes until the 16.2 km where the leftmost lane drops. At 15.14 km an acceleration lane appears, so the network is composed again by four lanes. Furthermore, at the 11 km a lane is added to the network, until the end of the test site network. It includes eight on-ramps and seven off-ramps. In order to model the network by use of METANET, the freeway stretch is represented by 25 nodes (N0-N24) and 24 links (L1-L24), where each node corresponds to a bifurcation or a junction or any location marking a change of the network geometry; whereas the homogeneous road stretches between these locations are represented by links. Each network link is subdivided in segments of equal length, for the purposes of this thesis each segment is approximately 400 meters. For example, link L1 is divided in three segments, with the vertical short lines denoting the segment borders. Figure 4.2 displays the length, number of sections and number of lanes for each link, the exact location of the on-ramps and off-ramps, of the available detector stations which are depicted by black bullets and their name, as well as of the available variable speed limit gantries which are depicted by red bullets.
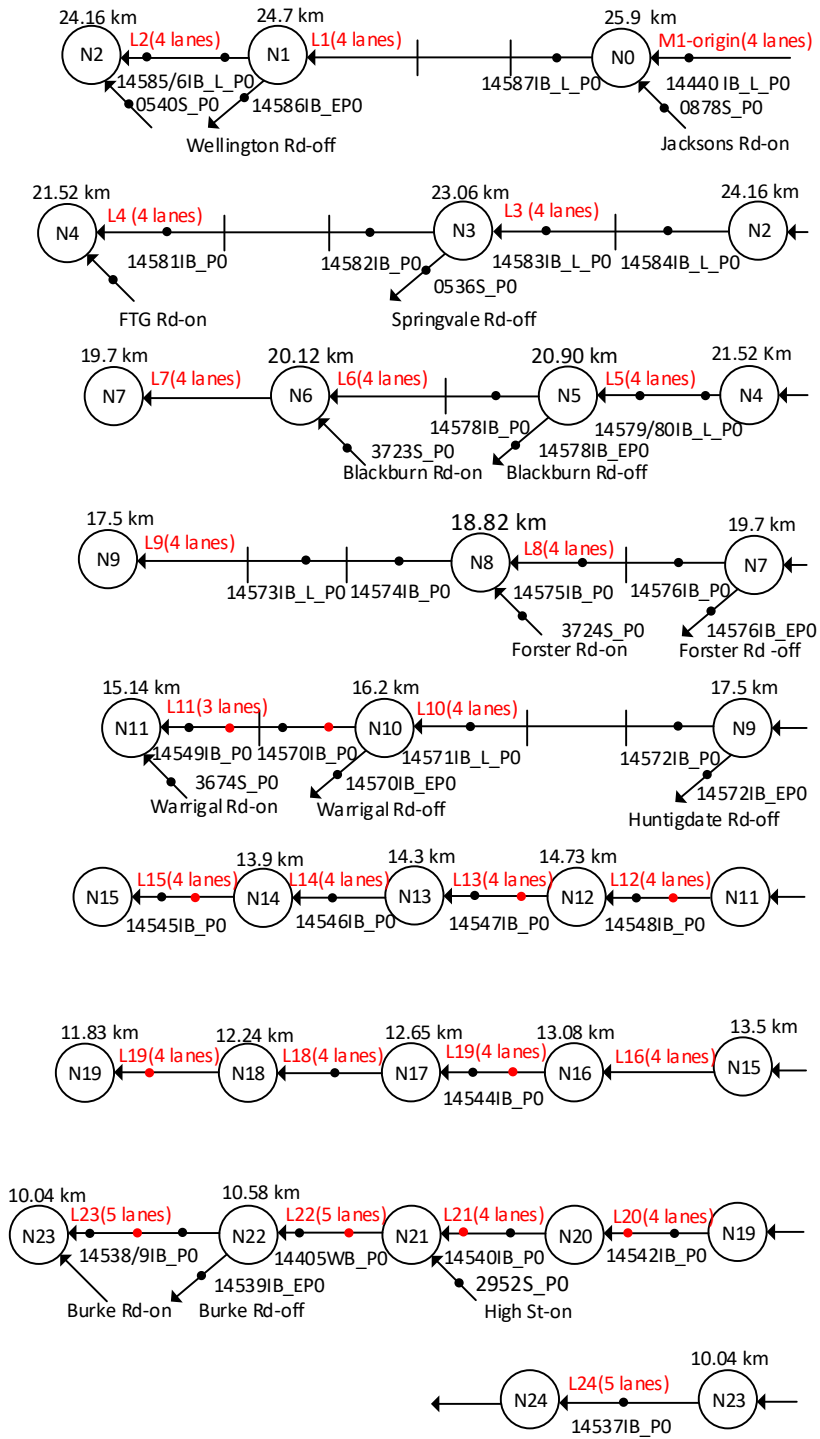
FIGURE 4.2: Representation of the considered freeway stretch

The described network is cautiously designed in our extended software tool CALISTO. This is a crucial point for calibration since intention is to decrease the deflection between the measured speed from the detectors in the real field and the macrosimulation model. Detectors delivering flow and speed measurements are available in the mainstream and at the on-ramps and off-ramps. Figure 4.2 illustrates the exact locations of the detectors in the simulation model, while Table 4.1 illustrates the dates that we have measurements of traffic flows and speeds. Flow measurements for the related on-ramps and off-ramps are illustrated in Figures A.3-A.6.

### 4.1.2 Real Traffic Conditions

The proximity of the model output to the field data is quantified by mainly the speed measurements. As a matter of fact, during calibration we aim to set up the simulator so as to reproduce speeds as close as possible to the real ones. This will lead to the reproduction of real traffic conditions as well as of the exact location of congestion points (bottlenecks) . In order to determine which day's data is going to be utilized for the calibration procedure, we need to observe the conditions that occur each day and then decide which datasets are the most suitable for our study case.

Figures 4.3 - 4.8 represent the speeds measured from the detectors placed along the examined network for all the days we have available data. On the left side of each figure the names of on-ramps are specified. The horizontal axis represents the time horizon (hour) and on the right side of the graph it is specified which color corresponds to different speed measurements.
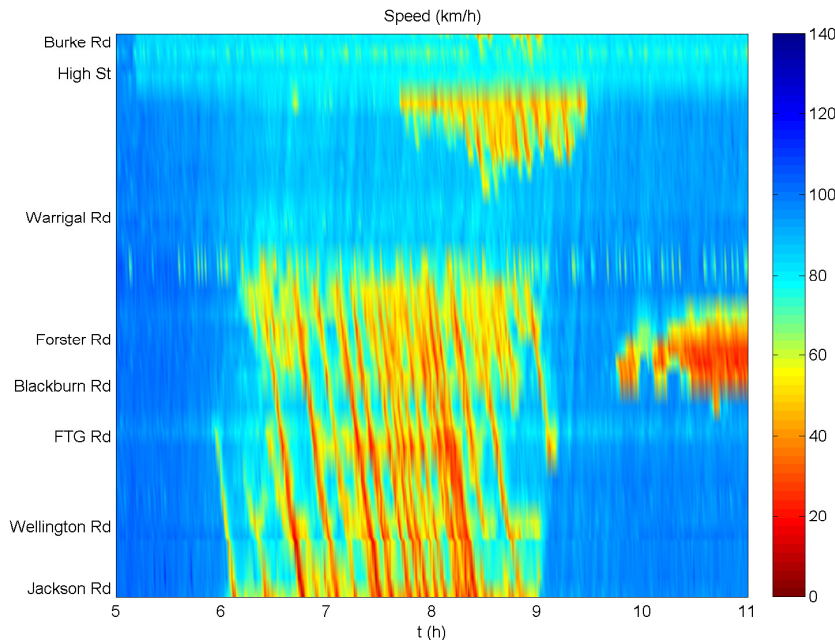


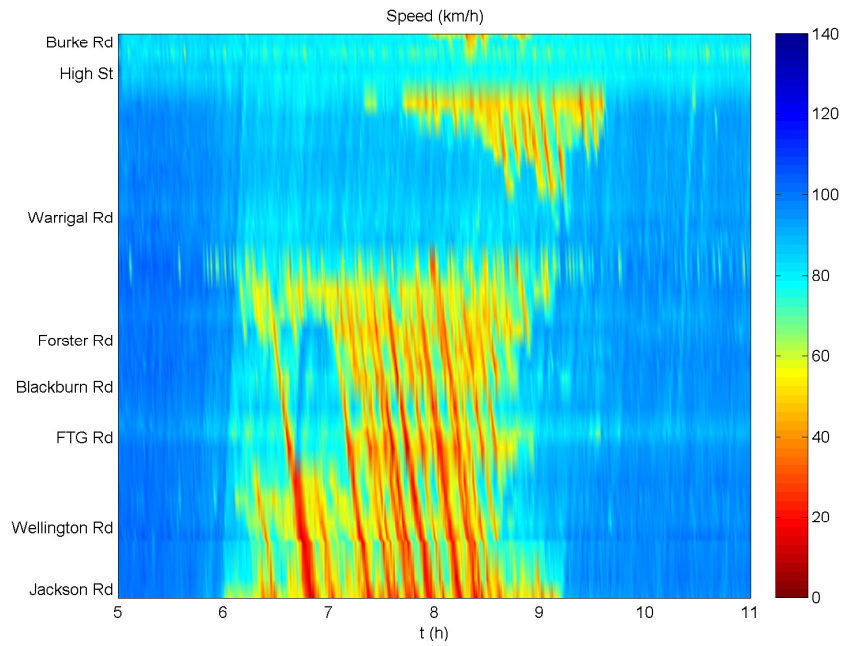FIGURE 4.3: Real speed data for Monday 15-08-2016

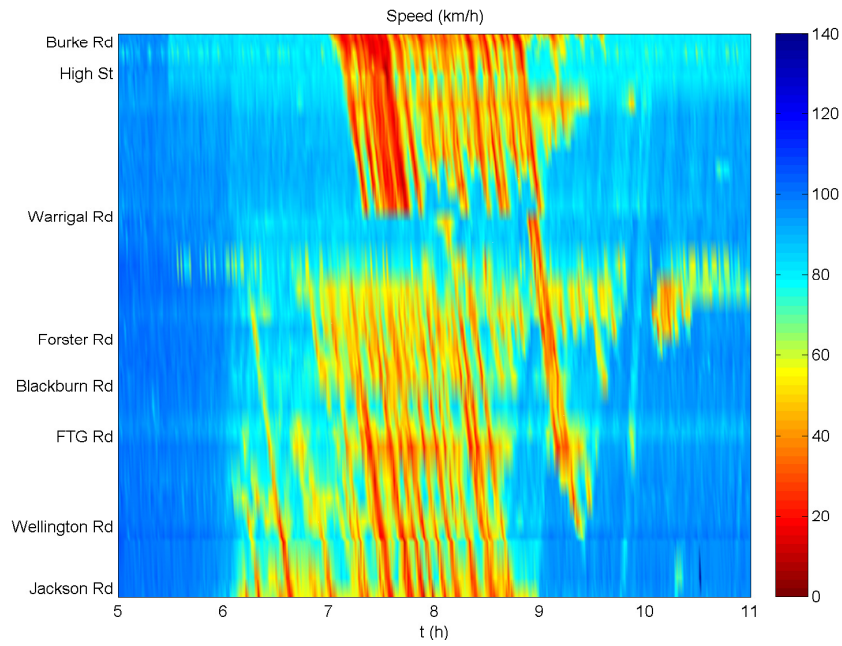FIGURE 4.4: Real speed data for Tuesday 16-08-2016



FIGURE 4.5: Real speed data for Thursday 18-08-2016
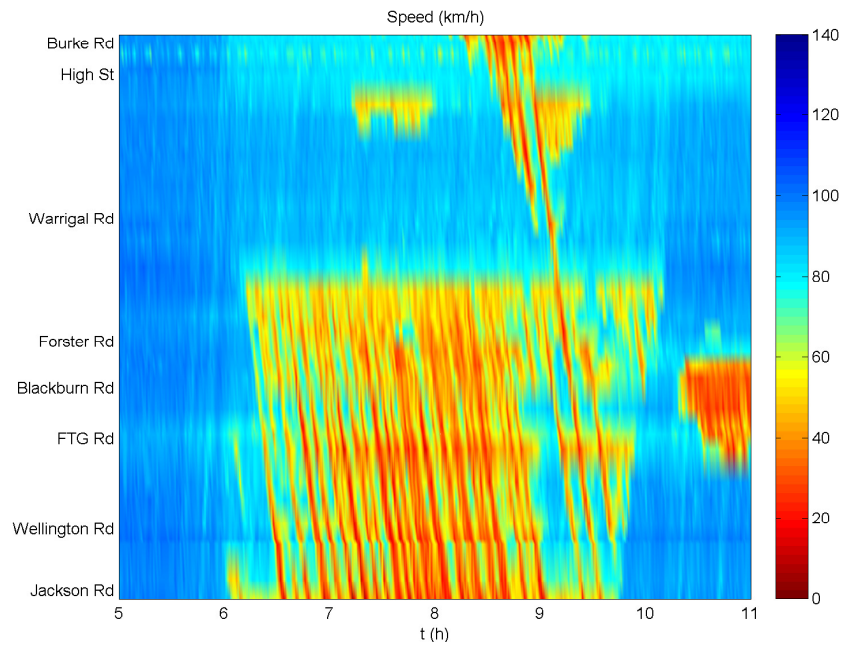
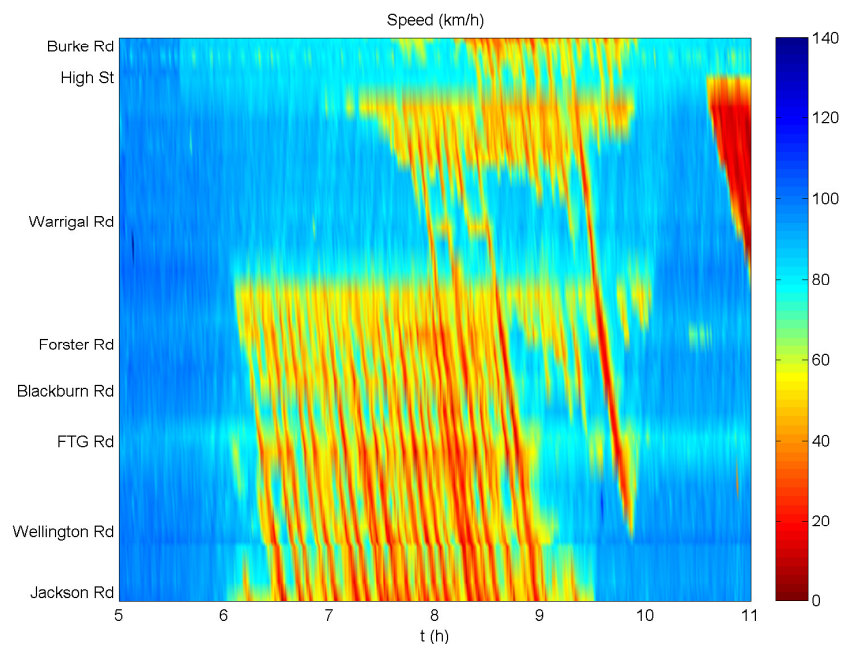FIGURE 4.6: Real speed data for Tuesday 8-11-2016



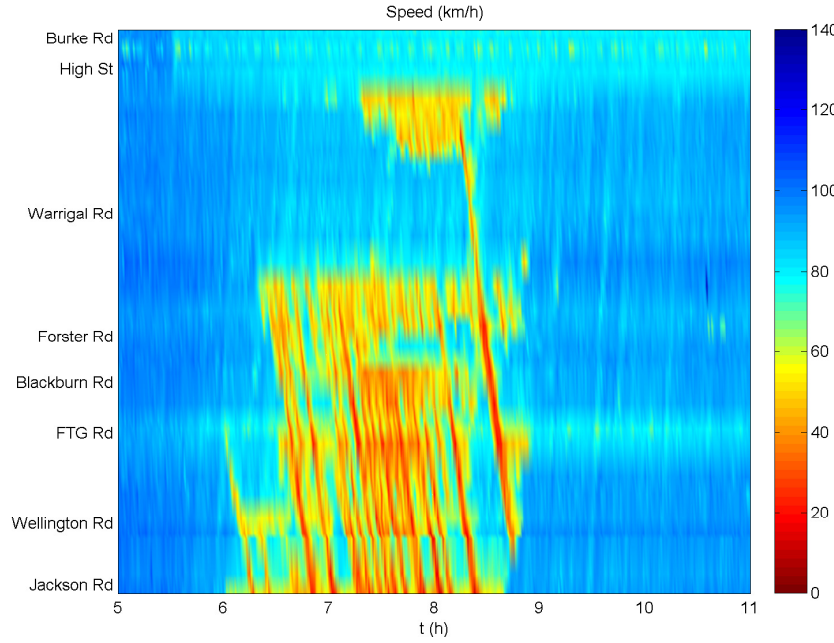FIGURE 4.7: Real speed data for Wednesday 9-11-2016

FIGURE 4.8: Real speed data for Friday 11-11-2016

The congestion pattern for the network can be extracted from the speed measurements demonstrated in the above figures for each day:

- **Monday 15/08/2016 :** Congestion appears first at 6:25 AM upstream of the Warrigal Rd off-ramp (L10 in Figure 4.2) due to weaving and spills back covering the upstream motorway stretch lasting until almost 9:00 AM. A second congestion is formed at around 8:00 AM upstream of the High St area (L20 in Figure 4.2) again due to weaving. This phenomenon spills back to the merge area of the Warrigal Rd on-ramp and lasts until 9:30 AM. Finally, there is another congestion initiated at the merge area of the Forster Rd on-ramp (L9 in Figure 4.2) that spills back to the FTG Rd area and ends after 11:00 AM, i.e. outside of the time window considered in this study.

- **Tuesday 16/08/2016:** At this day two different congestions occur throughout the six-hour period considered. The first appears at 06:25 AM upstream of the Warrigal Rd off-ramp (L10 in Figure 4.2) and spills back covering all the upstream network, lasting until 08:30 AM. A second congestion is formed at 08:00 AM until 09:30 AM and is created upstream of the High St area (L20 in Figure 4.2). This traffic jam spills back to the merge area of the Warrigal Rd on-ramp.

- **Thursday 18/08/2016:** The speed contour plot of this day illustrates partly similar traffic conditions to the ones of *Tuesday 16/08/2016*. The two bottlenecks interfere with each other and this results to a longer duration of the congestion from 06:00 AM until almost 10:00 AM. The first congestion appears from 06:00 AM upstream of the Warrigal Rd off-ramp (L10 in Figure 4.2) and spills back

covering all the upstream network.  As it concerns the second congestion, it is
formed at 07:15 AM downstream of the Burke Rd area (L20 see Figure 4.2) and
merges with the first congestion point downstream the Warrigal Rd of-ramp at
around 09:30 AM.

- **Tuesday 08/11/2016:** The traffic pattern of this day consist of a bottleneck start-
  ing at 06:00 AM upstream of the Warrigal Rd off-ramp (L10 in 4.2) due to strong
  weaving and spills back covering all the upstream motorway stretch lasting
  until almost 10:00 AM. A second moving traffic jam appears at 08:30 AM and
  steams from the area downstream of Burke Rd. This phenomenon spills back
  to the merge area of the Warrigal Rd on-ramp and lasts until 09:30 AM. Finally,
  there is another congestion initiated at the merge area of the Forster Rd on-
  ramp (L9 in Figure 4.2) that spills back to the upstream of the FTG Rd area and
  ends after 11:00 AM.

- **Wednesday 09/11/2016:** The speed contour plot for this day illustrates similar
  traffic conditions to the ones of *Tuesday 8/11/2016* as it concerns the congestion
  which is formed upstream of the Warrigal Rd off-ramp (L10 in Figure 4.2).  A
  second congestion point is initiated at around 07:30 AM downstream the Burke
  Rd area due to weaving (L23 in Figure 4.2). This phenomenon spills back to the
  merge area of the Forster Rd and lasts until 10:00 AM. Finally, there is another
  congestion initiated at the merge area of the High St on-ramp (L21 in Figure
  4.2) that spills back upstream of the Warrigal Rd area and ends after 11:00 AM,
  i.e. outside of the time window considered in this study.

- **Friday 11/11/2016 :** The congestion pattern of this day is quite clear.  The first
  bottleneck appears at around 06:30 AM upstream of the Warrigal Rd off-ramp
  (L10 in Figure 4.2) due to weaving and spills back covering all the upstream
  network. The main sources of the traffic jam is increased demand of the drivers
  to turn at the Warrigal Rd off-ramp. A second congestion is formed at around
  07:30 AM upstream of the High St area (L20 in Figure 4.2) again due to weav-
  ing.  This phenomenon spills back to the merge area of the Warrigal Rd on-
  ramp and lasts until almost 09:00 AM.

One of the main uses of a calibrated model is the development and testing of
control algorithms.  In order to select the most appropriate days for the calibration
and validation procedures, it will be good to avoid phenomena initiated out of the
considered boundaries of the motorway stretch. This is because these kinds of phe-
nomena are not easily treated by any control algorithm. Based on the above rational,
the datasets that can be used for the model's calibration are eliminated to the follow-
ing:

- Monday 15/08/2016

- Tuesday 16/08/2016

- Friday 11/11/2016

Eventually, the parameters of the simulation model will be tuned in order to replicate traffic conditions of *Friday 11/11/2016*. The observed speeds will be used in order to evaluate the model's performance. Similarly, the datasets of the rest days will be used in order to validate the model.

## 4.2 Calibration and Validation

### 4.2.1 Parameter Setup

In the first stage of the calibration we adjusted information about the freeway network description. We specified the number of mainstream links, the number of off-ramps and on-ramps which included in the simulated freeway stretch. Also information about the number of detector stations, the number of the lanes at the entrance and at the exit, the number of sections per link and the link's length is given. In addition, the location of each on-ramp and off-ramp is defined. Finally, a table with all the names of variable speed limits stations which are implemented in each link is illustrated in the *Freeway Network Description* window of CALISTO.

In addition, an excel file which contains all the information about the examined network is adjusted. Every excel-sheet contains different data sets. For example the first excel-sheet consist of the main traffic flow measurements, with measurements interval equal to 60 seconds, and every column corresponds to a different detector. A second excel-sheet contains information about the measured speeds from each detector respectively. Also in different excel-sheets the traffic flow and speed measurements at the boundary locations are given. In addition, information about the flow and speed for every on-ramp and every off-ramp are included in the excel file. For the purposes of this thesis, one more excel-sheet has been added, which contains information about the variable speed limits applied at each section of the examined network stretch.

Moreover, some general parameters of the model are adjusted. These parameters are the simulation step $T$=10 sec, the weigh error for the speed, $w_s$=1 and the weigh error for the flow, $w_f$=0. In addition, the selected traffic flow model as already mentioned is the second order model namely, METANET. CALISTO requires the specification of the three following categories of METANET parameters in order to calibrate the network:

1. **Global Parameters**: concern all vehicles independent of their type and the section of the network they are driving.

2. **Group links with common FD**: the network is discretized in different sections with respect to the geographical characteristics and their infrastructure.

3. **FD parameters per group**: in each group the parameters $v_f$, $\rho_{cr}$, $\alpha$, $A$ and $E$ are specified, and they are the same for all links in each group.

It worths to say that various calibration tests were carried out using different initial values for the parameters. The first set of them is illustrated in tables 4.2-4.3. To begin with, in Table 4.2 the initial values of the global parameters are presented. The last two parameters, in particular $\kappa$ and $v_{min}$ are not calibrated.

| Parameter | Initial Value |
|:---:|:---:|
| $\tau$(sec) | 10 |
| v($km^2$/h) | 15 |
| $\delta$ (h/km) | 0.200 |
| $\phi$ (h/km) | 0 |
| $\kappa$ (veh/km/lane) | 10 |
| $v_{min}$(km/h) | 7 |

TABLE 4.2: Global parameters

As it concerns the FD parameters per group, these are illustrated in table 4.3. The parameters $A$ and $E$ are fixed which means that Nelder-Mead doesn't search an optimum value for them. The reason for keeping these parameters constant is that the VSLs displayed, in the biggest part of the freeway stretch are equal to the nominal speed. The only exceptions are two links (L22-L23 in Figure 4.2) where the displayed VSLs are 80km/h (Figures B.1-B.3), and on Friday 11-11-2016 (calibrated day), where five VMSs gantries (links 17, 15, 13, 12, 11 in Figure B.1) displayed speed equal to 60 km/h, just for a few seconds in the morning hours, in particular in 08:10 AM. As it is obvious, the parameter $b$, that is the ratio between the displayed speed and the nominal speed, is one for the biggest part of our measurements. As a result, the calibrated outcome is independent from the values of the parameters $A$ and $E$. The optimizer, in order, to reproduce the optimum result, for L22-L23, makes various combinations with the values of the parameters $A$ and $\rho_{cr}$ which are however correlated (see 2.11). Also the parameters $E$ and $\alpha$ are correlated (see 2.12). In order to avoid, that correlation we decide to set the parameters $A$ and $E$ fixed, [16].

| Groups | Links | $v_f$(km/h) | $\rho_{cr}$(veh/km/lane) | $\alpha$ | $A$ | $E$ |
|--------|-------|-------------|--------------------------|----------|--------|--------|
| Group 1 | 1-9 | 100 | 31 | 2 | 0.3333 | 1.8226 |
| Group 2 | 10 | 100 | 32 | 2 | 0.3333 | 1.8226 |
| Group 3 | 11-19 | 100 | 42 | 2 | 0.3333 | 1.8226 |
| Group 4 | 20-21 | 100 | 32 | 2 | 0.3333 | 1.8226 |
| Group 5 | 22-25 | 100 | 35 | 2 | 0.3333 | 1.8226 |

TABLE 4.3: FD parameters per group

Table 4.4 illustrates the selected values for the Nelder-Mead algorithm. In the final step it was specified that the selected operation is the *Calibration*, where it calibrates the METANET model, using the Nelder-Mead algorithm, for the particular freeway network, using the defined traffic data.

| Parameter's name | Parameter's Value |
|------------------|-------------------|
| Tol.fun | 1.0000e-03 |
| Tol.x | 1.0000e-03 |
| Max.iter | 1000 |

TABLE 4.4: Nelder-Mead parameters

### 4.2.2 Calibration Results

Throughout the calibration procedure, the sum of squared errors between the simulated and the observed speed is the index to be minimized (Equation 3.2). In the following, the optimization results of the utilized algorithm are presented, followed by the multiple combinations that were tested in order to take the optimum result.

To begin with, Table 4.5 presents the calibration results of the first calibration test. The selected parameter's values examined for five calibration runs and the results are the following.

| Calibration run | Iterations | Performance Index |
|:---:|:---:|:---:|
| 1 | 1000 | 13.1734 |
| 2 | 1000 | 12.1265 |
| 3 | 1000 | 12.1356 |
| 4 | 1000 | 12.1356 |
| 5 | 1000 | 13.2295 |

TABLE 4.5: Nelder-Mead algorithm; performance criteria

Note that, in these calibration tests the only FD parameters that were not cali-brated are the $A$, $E$. As it concerns the global parameters only $\kappa$ and $v_{min}$ remained fixed. As a consequence, the Nelder-Mead algorithm found the optimum values for the rest of the parameters, which have been calibrated. It should be specified that the values for the parameters $v_f$, $\rho_{cr}$ and $\alpha$ were indicated for each group, and they may be different. As a second calibration test in order to find the optimum result, we used the average values of $v_f$ and $\rho_{cr}$ for each group, from the previous calibration runs. In addition, we set them fixed and we did again the calibration procedure. The average values per group, for the previously mentioned parameters, as well as the fixed values for VSL's parameters and the initial values for the parameter $\alpha$, are presented in Table 4.6

| Group | $v_f$(km/h) | $\rho_{cr}$(veh/km/lane) | $\alpha$ | $A$ | $E$ |
|:---:|:---:|:---:|:---:|:---:|:---:|
| 1 | 100 | 31 | 2 | 0.3333 | 1.8226 |
| 2 | 105 | 32 | 2 | 0.3333 | 1.8226 |
| 3 | 100 | 40 | 2 | 0.3333 | 1.8226 |
| 4 | 95 | 32 | 2 | 0.3333 | 1.8226 |
| 5 | 105 | 34 | 2 | 0.3333 | 1.8226 |

TABLE 4.6: The average value of the calibrated parameters with the VSL's parameters

The performance index of the various calibration runs are illustrated in Table 4.7, while the results of the best calibration test are illustrated in Tables 4.8 and 4.9. As already has mentioned, the parameters $\kappa$ and $v_{min}$ have not been calibrated, that is the reason why they remained the same as before the calibration procedure.

| Calibration run | Iterations | Performance Index |
|:---:|:---:|:---:|
| 1 | 140 | 13.9717 |
| 2 | 450 | 12.449 |
| 3 | 900 | 12.587 |
| 4 | 1000 | 12.5462 |
| 5 | 580 | 12.4986 |

TABLE 4.7: Nelder-Mead algorithm; performance criteria

| Parameter | Calibrated Value |
|:---:|:---:|
| $\tau$(sec) | 9.4568 |
| v(km$^2$/h) | 18.7998 |
| $\delta$ (h/km) | 0.2269 |
| $\phi$ (h/km) | 2.6325e-08 |
| $\kappa$ (veh/km/lane) | 10 |
| $v_{min}$(km/h) | 7 |

TABLE 4.8: Calibrated global parameters

| Group | $v_f$(km/h) | $\rho_{cr}$(veh/km/lane) | $\alpha$ | $A$ | $E$ |
|:---:|:---:|:---:|:---:|:---:|:---:|
| 1 | 100 | 31 | 2.1787 | 0.3333 | 1.8226 |
| 2 | 105 | 32 | 2.0400 | 0.3333 | 1.8226 |
| 3 | 100 | 40 | 2.0750 | 0.3333 | 1.8226 |
| 4 | 95 | 32 | 1.8648 | 0.3333 | 1.8226 |
| 5 | 105 | 34 | 2.0046 | 0.3333 | 1.8226 |

TABLE 4.9: Calibrated FD parameters

With regard to the *Cost function evaluation* and the contour plot the best *Calibration run* in number 5 (see Table 4.7). The traffic conditions produced by the calibrated model are illustrated in Figure 4.10 while for the sake of completeness the real data speed is shown again in Figure 4.9 .
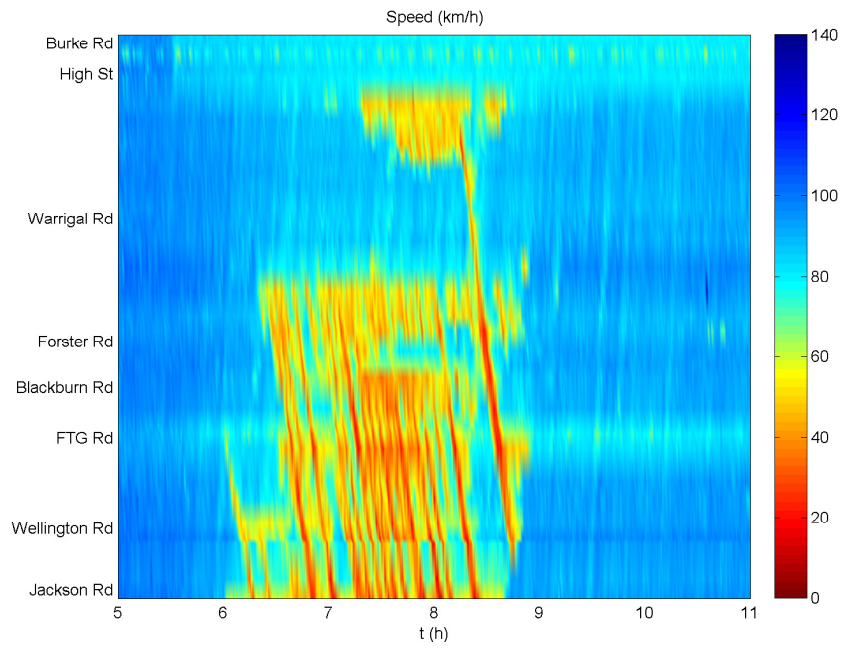
FIGURE 4.9: Real Traffic Speed Friday 11-11-2016 05:00-11:00 AM
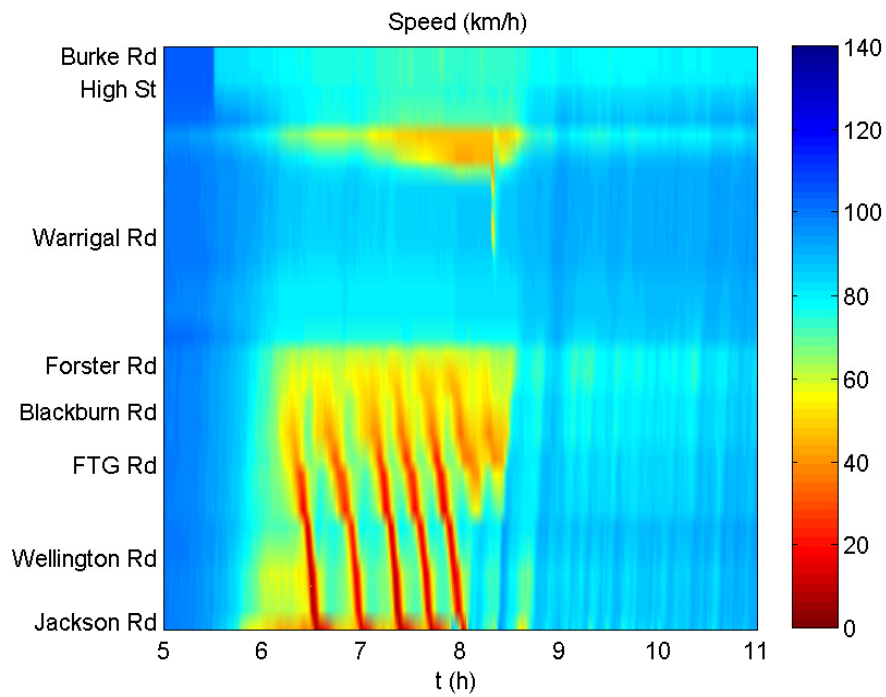


FIGURE 4.10: Simulated Speed Friday 11-11-2016 05:00-11:00 AM

The first bottleneck appears due to strong weaving upstream of the Warrigal Rd off-ramp and spills back covering all the upstream network. Our model, reproduces this phenomenon just downstream the on-ramp Forster Rd. The main reason for this result, is the difficulty that our model faces to replicate congestion after an off-ramp, while the lanes of the motorway stretch remain the same. The traffic jam seems to be created at the same time as in the real life network. The duration that bottlenecks appear as well as the extent of the congestion spill-back are in good agreement with reality. The second congestion point seems to be in a good agreement with the real traffic conditions, as concerns the location of the phenomenon. In the simulated data the congestion seems to start at around 06:30 AM, while in real traffic conditions the congestion firstly appears at 07:30 AM. In both cases the bottleneck lasts until 09:00 AM.

The detector locations were previously demonstrated in Figure 4.2 and below the aggregated flows and speeds measured as well as the computed densities at each one of the locations are presented at Figures 4.11-4.22. The red lines illustrate the flow produced by the macroscopic model while the black lines concerns the real data traffic flows,speeds and densities. Except from some minor portions of the network, the simulated flow is similar to the real flow measurements. Most importantly, it is apparent that the model is capable of reproducing the capacity-drop phenomena. This drop of the outflow firstly appears at *Detector location 9* which is before the off-ramp Hundigdate Rd. where congestion is triggered. A second crucial location in *Detector location 22-23* where the simulated flow is not reproduced with great accuracy, but as it is obvious at the final two links the simulated flow is quite similar to the real flow measurements. As a consequence, the main reason of this phenomenon, are wrong measurements from a probably not accurate detector.
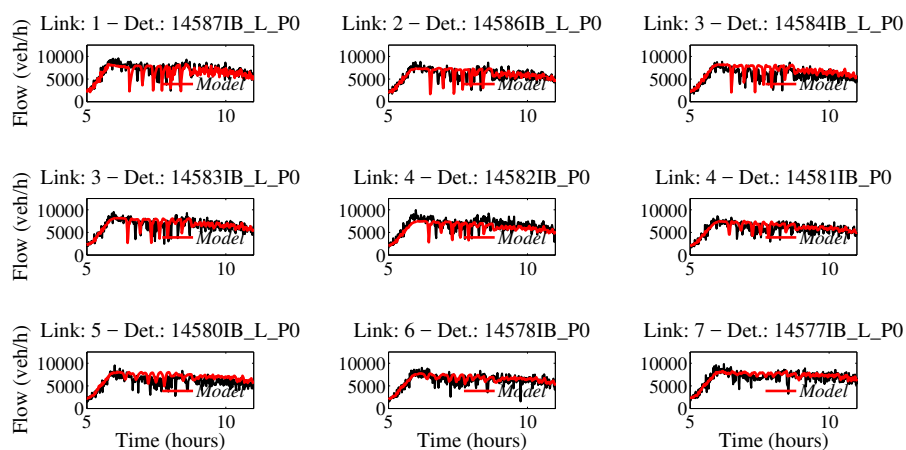


FIGURE 4.11: Comparison between measured (black line) and simulated (red line) aggregate flow at detector locations 1-7
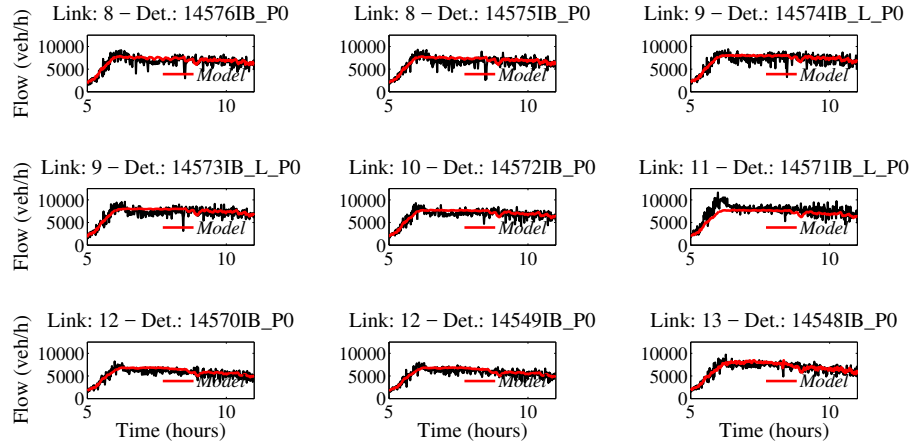
FIGURE 4.12: Comparison between measured (black line) and simulated (red line) aggregate flow at detector locations 8-13
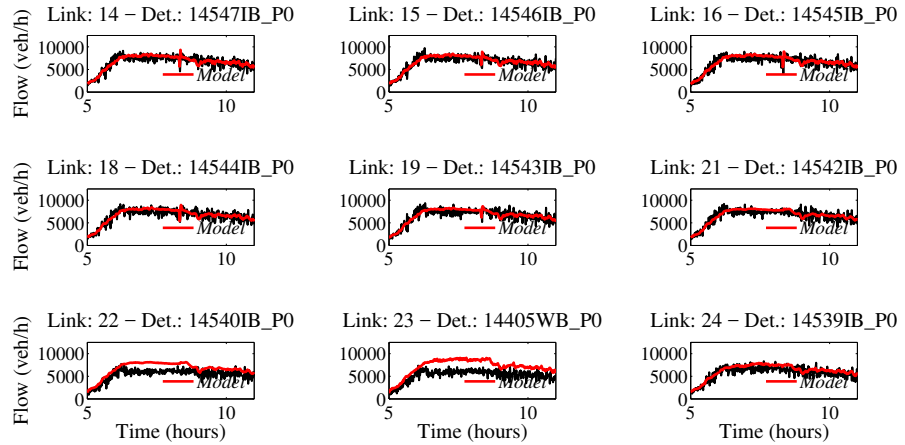


FIGURE 4.13: Comparison between measured (black line) and simulated (red line) aggregate flow at detector locations 14-24
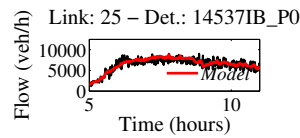


FIGURE 4.14: Comparison between measured (black line) and simulated (red line) aggregate flow at detector location 25
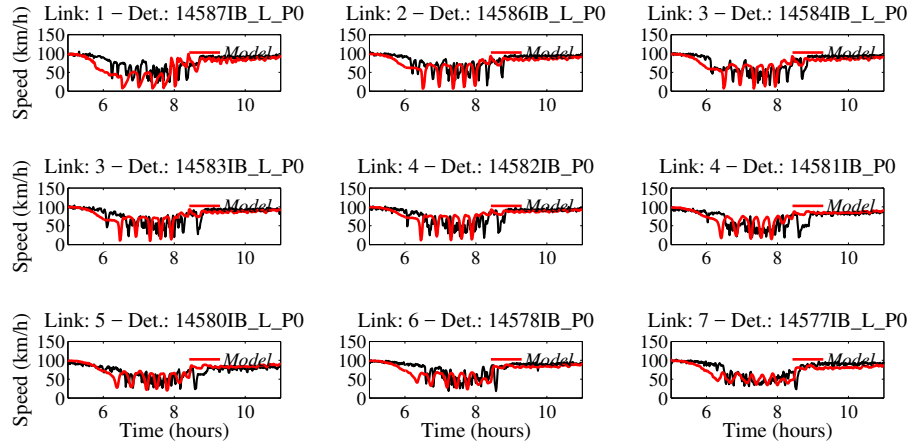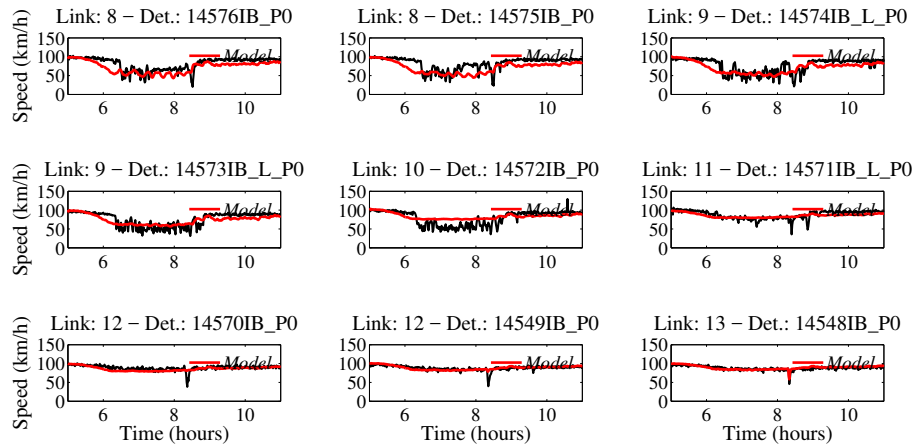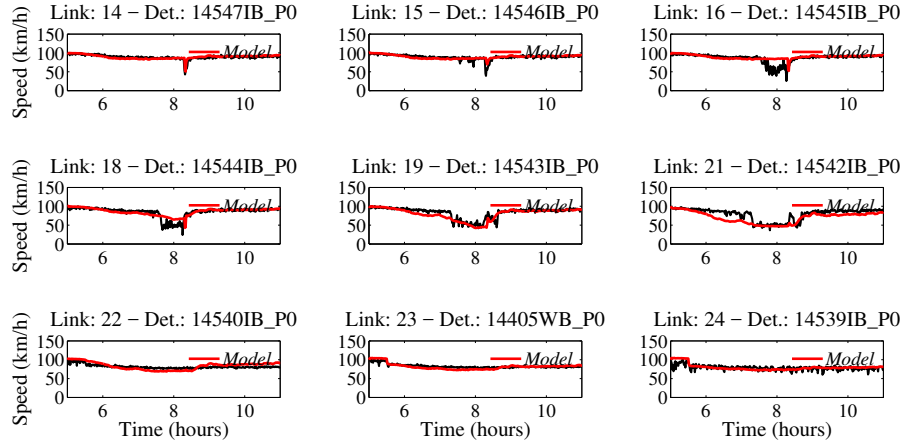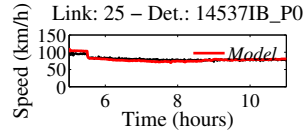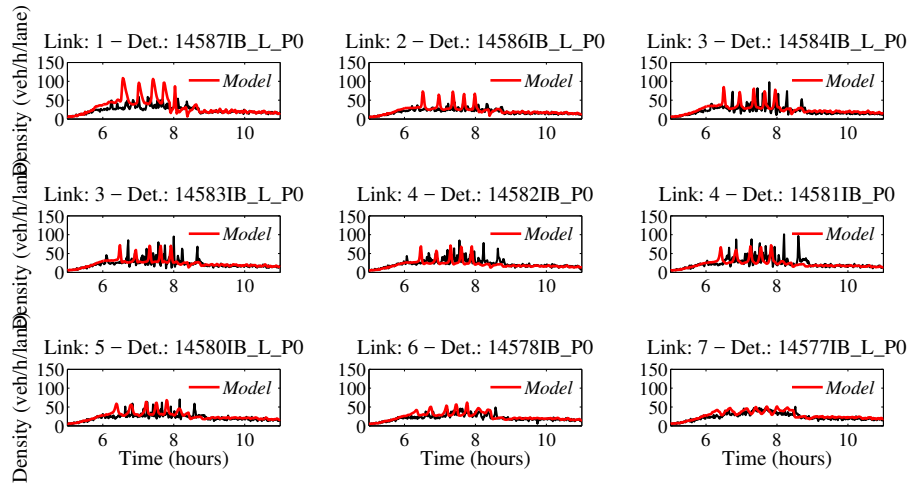
FIGURE 4.15: Comparison between measured (black line) and simulated (red line) aggregate speed at detector locations 1-7
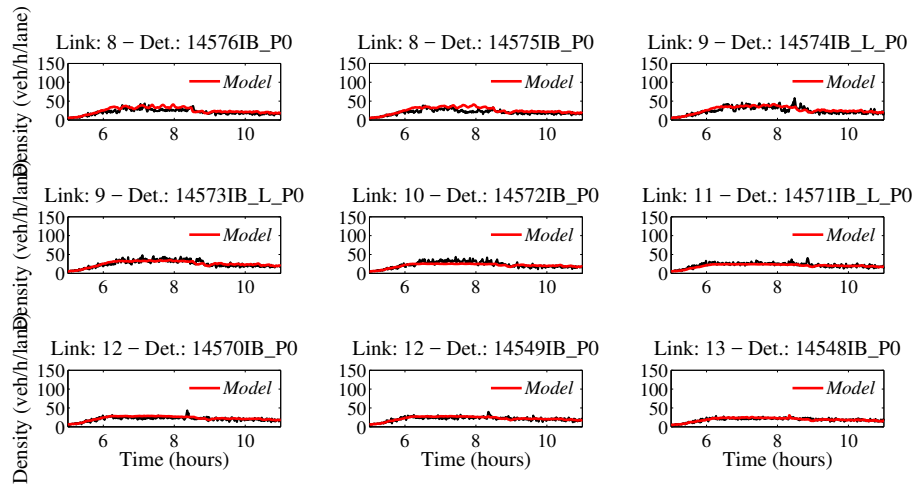


FIGURE 4.16: Comparison between measured (black line) and simulated (red line) aggregate speed at detector locations 8-13

FIGURE 4.17: Comparison between measured (black line) and simulated (red line) aggregate speed at detector locations 14-25



FIGURE 4.18: Comparison between measured (black line) and simulated (red line) aggregate speed at detector location 25
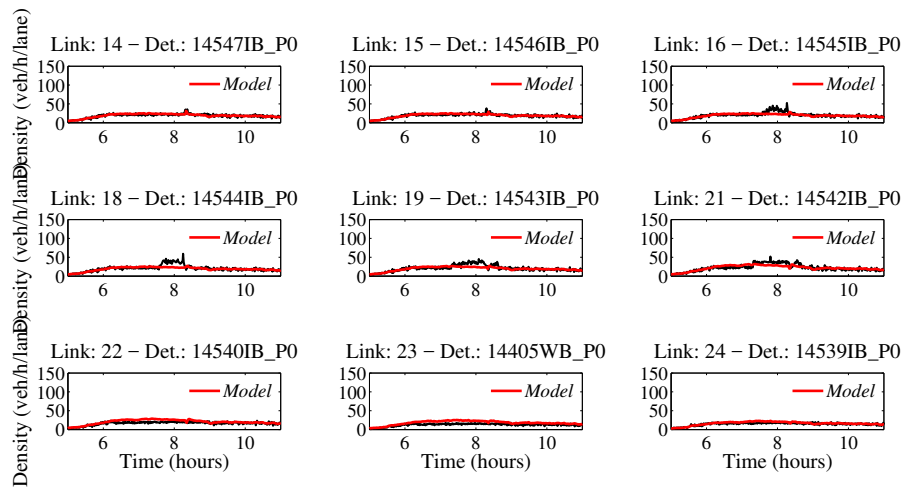


FIGURE 4.19: Comparison between computed (black line) and simulated (red line) aggregate density at detector locations 1-7

FIGURE 4.20: Comparison between computed (black line) and simulated (red line) aggregate density at detector locations 8-13



FIGURE 4.21: Comparison between computed (black line) and simulated (red line) aggregate density at detector locations 14-24
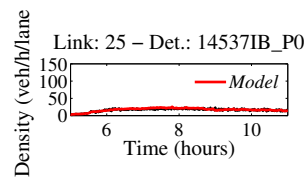


FIGURE 4.22: Comparison between measured (black line) and computed (red line) aggregate density at detector location 25

Finally, the graph of the calibration process over iterations is shown in Figure 4.23 (calibration run 5 see Table 4.7). It indicates that the best Performance Index is 12.4986 and the number of iterations that the algorithm executed is five-hundred eighty.
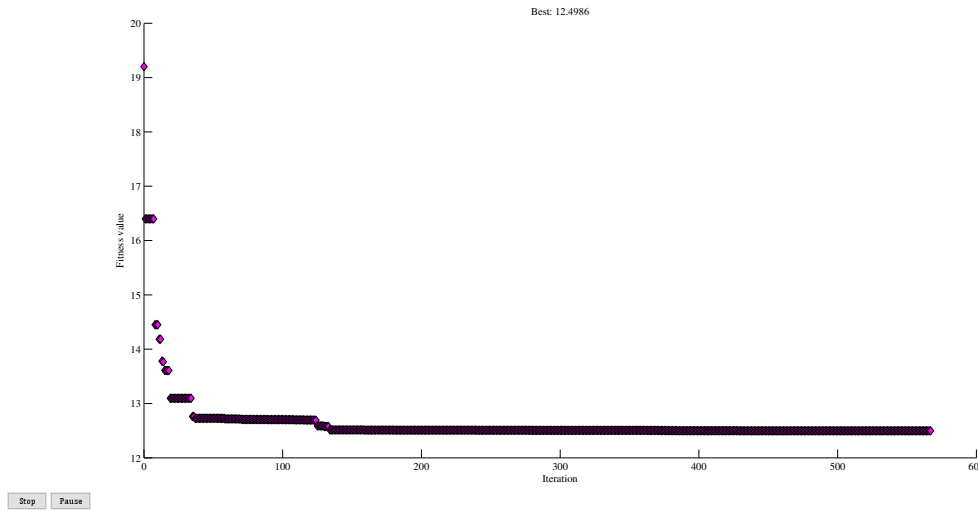


FIGURE 4.23: Output plot; best PI value over iterations.

### 4.2.3  Validation results

The purposes of the validation is to confirm that the calibrated model can replicate real life traffic scenarios under other conditions as well. To this end, different demand profiles are set based on the the field data collected on different days. The performance measure for the validation is again the speed measured across the network. Below, the traffic pattern produced by the calibrated model is compared to the real traffic conditions of each one of the selected days, which are Monday 15-08-2016 and Tuesday 16-08-2016.

- **Monday 15-08-2016:** The traffic conditions produced by the simulator, approach the reality quite well. Congestion is activated due to the strong weaving and spills back covering all the upstream network. The validated results illustrate the congestion downstream the on-ramp Forster Rd, while in reality congestion initiated upstream of the Warrigal off-ramp. The duration of the validated traffic congestion is the same as in reality. The second congestion point, which as already mentioned is formed upstream of the High St area seems to be in a good agreement with the validated results at it concerns the initiated location and the duration of the phenomenon. Although, the congestion in the validated results is quite stronger than in reality. Finally, the third traffic jam which is located downstream the Forster Rd area, is not reproduced by the simulator.
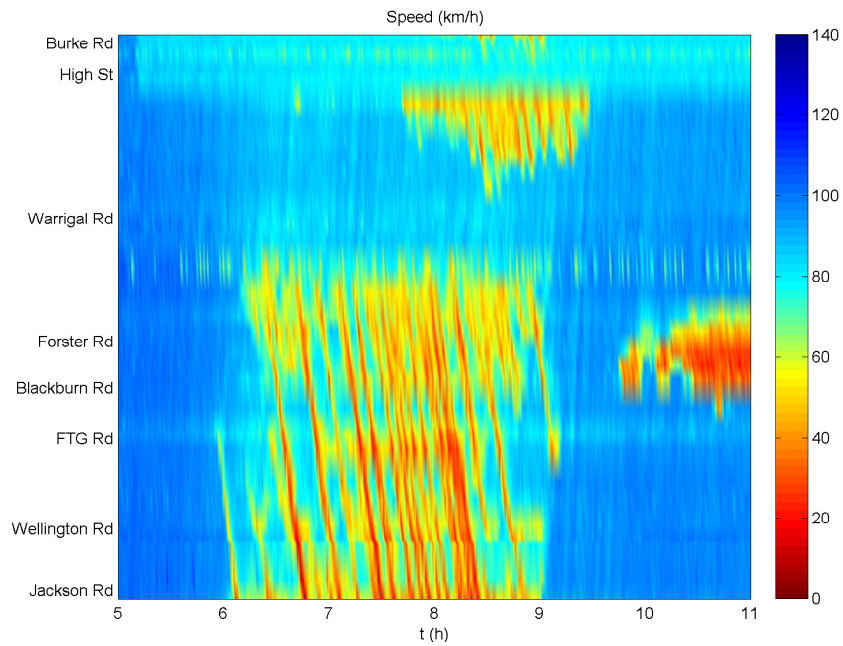
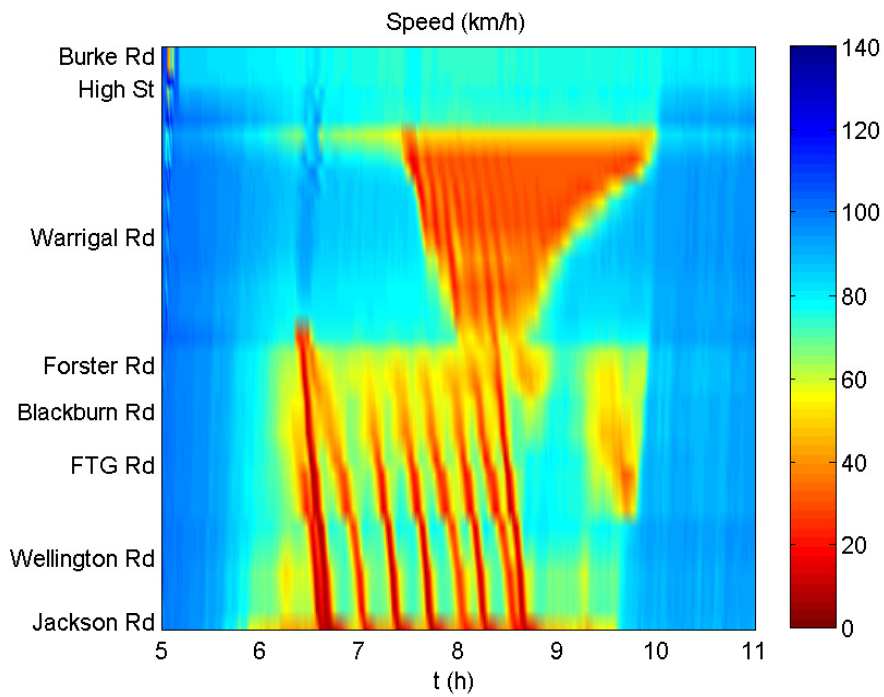FIGURE 4.24: Real data speed Monday 15-08-2016



FIGURE 4.25: Simulated speed, Monday 15-08-2016

- **Tuesday 16-08-2016 :** The calibrated model sufficiently replicates the traffic
conditions of this day. The validated results illustrate the congestion down-
stream the on-ramp Forster Rd, while in reality congestion initiated upstream
of the Warrigal off-ramp. The duration of the traffic jam as it is illustrated in
the validation results is one hour longer than in reality. The initial point, of
the second bottleneck totally matches with reality. Although, the congestion
seems to be much more stronger in the validated results and interfere with the
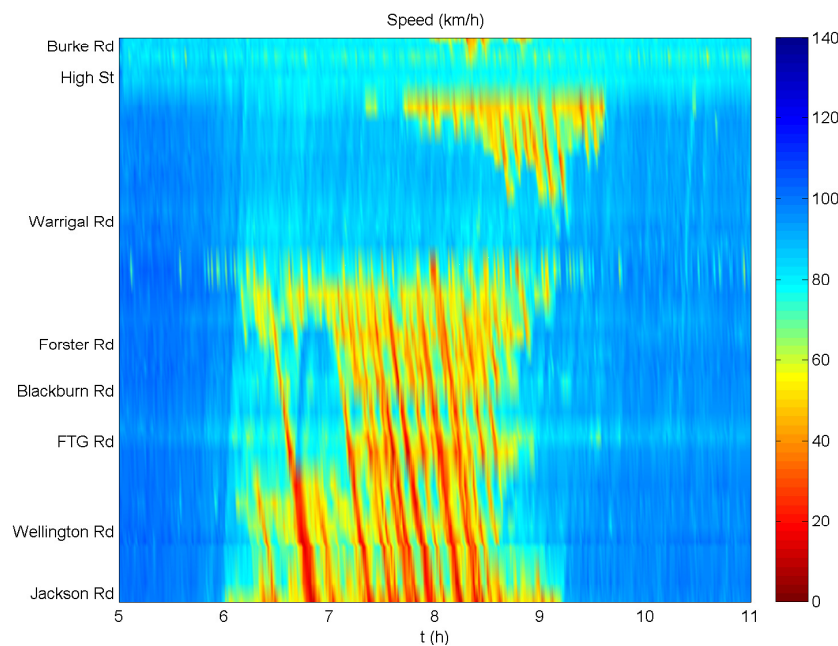Forster Rd merge area.



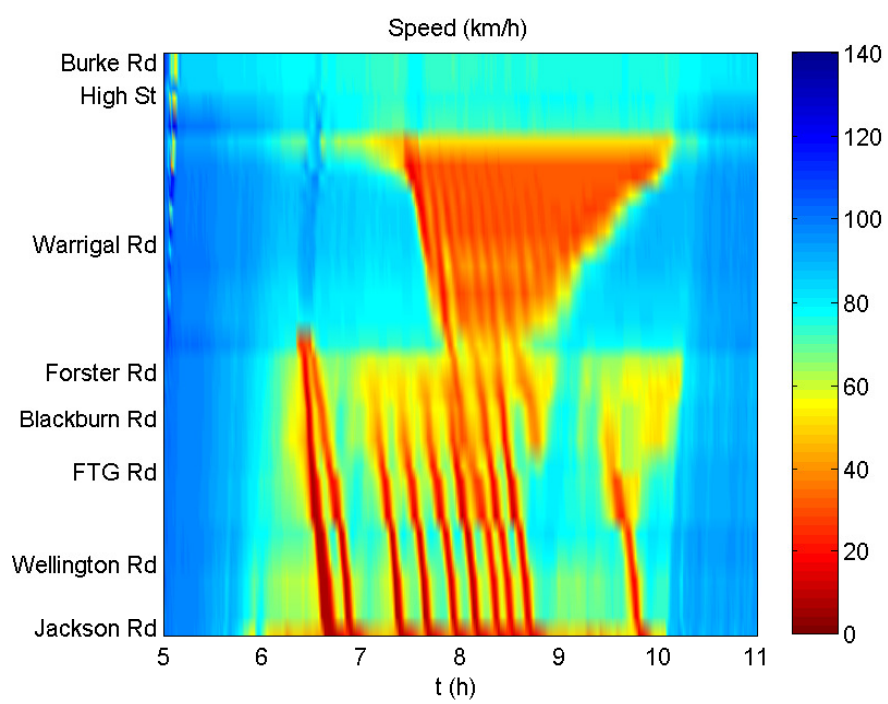FIGURE 4.26: Real speed, Tuesday 16-08-2016

FIGURE 4.27: Simulated speed, Tuesday 16-08-2016

# Chapter 5

# Conclusion and Future work

## 5.1 Conclusion

The objective of the diploma thesis was to calibrate a freeway stretch with variable speed limits (VSLs). To this end, a calibration and validation process was carried out using the extended CALISTO software tool. A second-order model was employed and examined, in particular the METANET model, using real traffic data. The model was examined regarding its ability to reproduce the prevailing traffic conditions on the motorway. In addition, the motorway was equipped with Variable Speed Limits (VSLs). The innovative software tool CALISTO was appropriately extended in order to handle VSLs and it was used for the calibration and validation procedure. CALISTO has been recently developed and makes the calibration and validation an easy task. In the utilized version of the software the examined model was programmed and introduced. Moreover, the software includes three optimization algorithms that that can be used for the calibration procedure, the Nelder-Mead algorithm, a genetic algorithm and the cross entropy method. The first optimization method was employed in the presented investigations. The case study site is a part of the freeway M1 which is located in Melbourne, Australia. The quite complex infrastructure features were developed with precision in the software tool while detailed traffic data flow and speed measurements were used in order to tune the macroscopic model parameters. It was proved that the selected parameters set in the macroscopic model can lead to realistic behavior. Not only the output speed pattern was well matched with the real one but also significant traffic phenomena were realistically replicated. The calibrated model was additionally validated and it was proved that the calibrated parameters can lead to acceptable performance.

## 5.2 Future Work

- Although this study has shown that the calibration of a motorway with complex infrastructure and the application of VSLs can lead to an accurate representation of the traffic conditions more VSL data need to be included to get further improvement on the overall performance.

- Moreover, the software tool CALISTO, could further be extended, by including more macroscopic traffic flow models, already existing or recently proposed, and also by including bigger selection of optimization algorithms.

- The presented model could be used for testing existing or new VSL control strategies that can handle congestion phenomena appearing simultaneously in different location of a network.

# Appendix A

# Appendix A

In this Appendix the graphs of the real flow measurements at the on-ramps and at the off-ramps are presented for the days used for calibration and validation. It is obvious, that the level of demand for the off-ramps at Burke and Warrigal road is increasingly high, for the examined hours. It should be noted that if the drivers want to take the exits mentioned above, should turn at the leftmost lane some kilometers upstream. This is the main reason for the formed congestion.

- Figures A.1 - A.2 illustrate the real traffic flows measured at the off-ramps and on-ramps respectively, on Friday 11-11-2016.

- Figures A.3 - A.4 illustrate the real traffic flows measured at the off ramps and on-ramps, on Monday 15-08-2016.

- Figures A.5 - A.6 illustrate the real traffic flows measured at the off ramps and on-ramps, on Tuesday 16-08-2016.
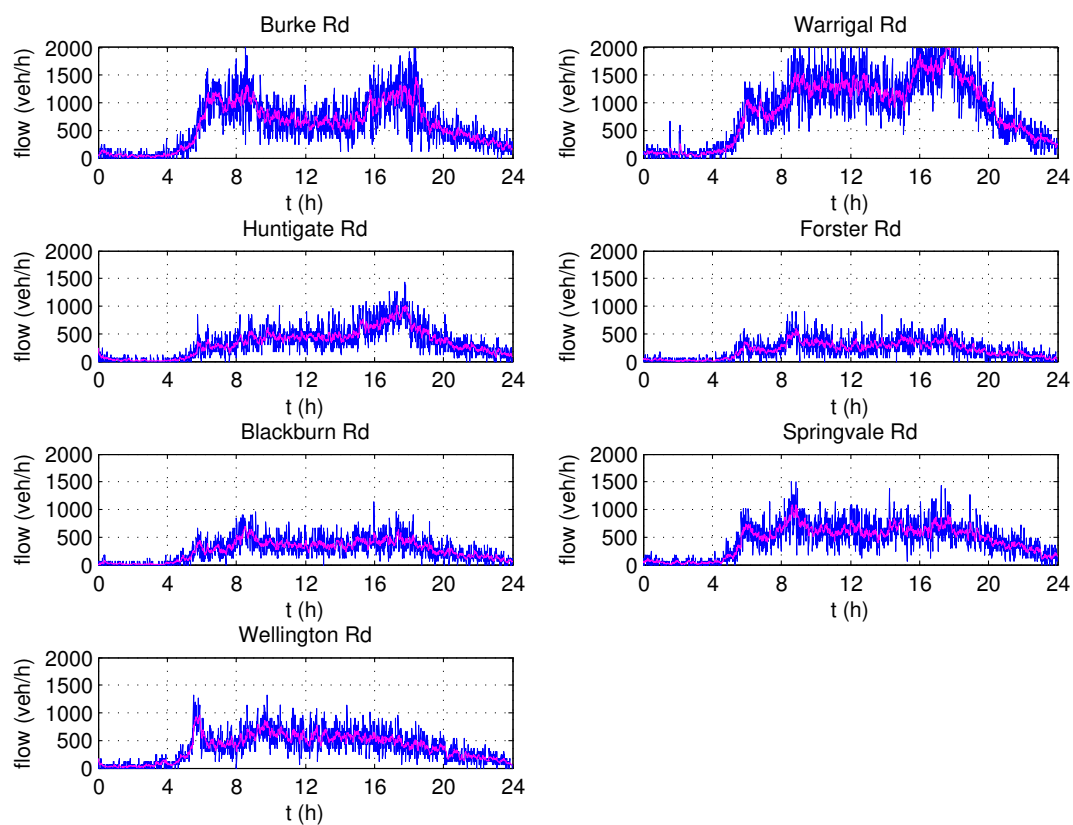
FIGURE A.1:   Comparison between measured (blue line) and smoothed (red line) flow at the off-ramps, Friday 11-11-2016
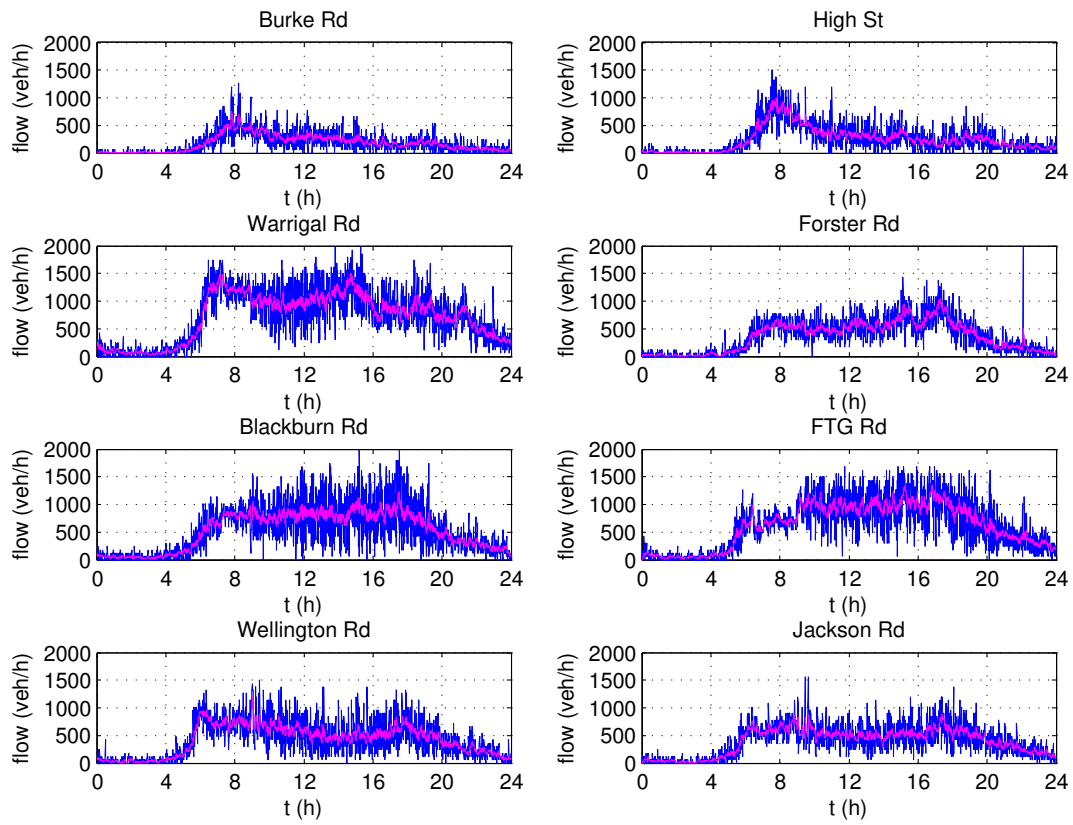
FIGURE A.2:   Comparison between measured (blue line) and smoothed (red line) flow at the on-ramps, Friday 11-11-2016
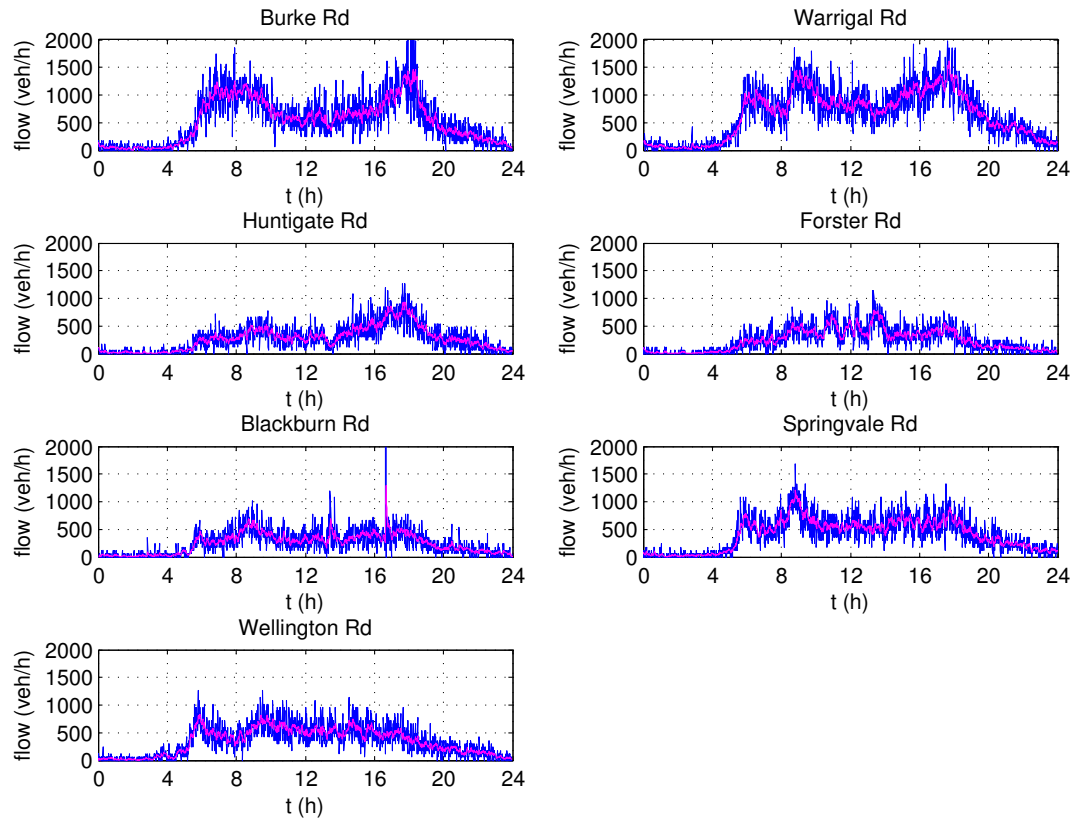
FIGURE A.3:    Comparison between measured (blue line) and
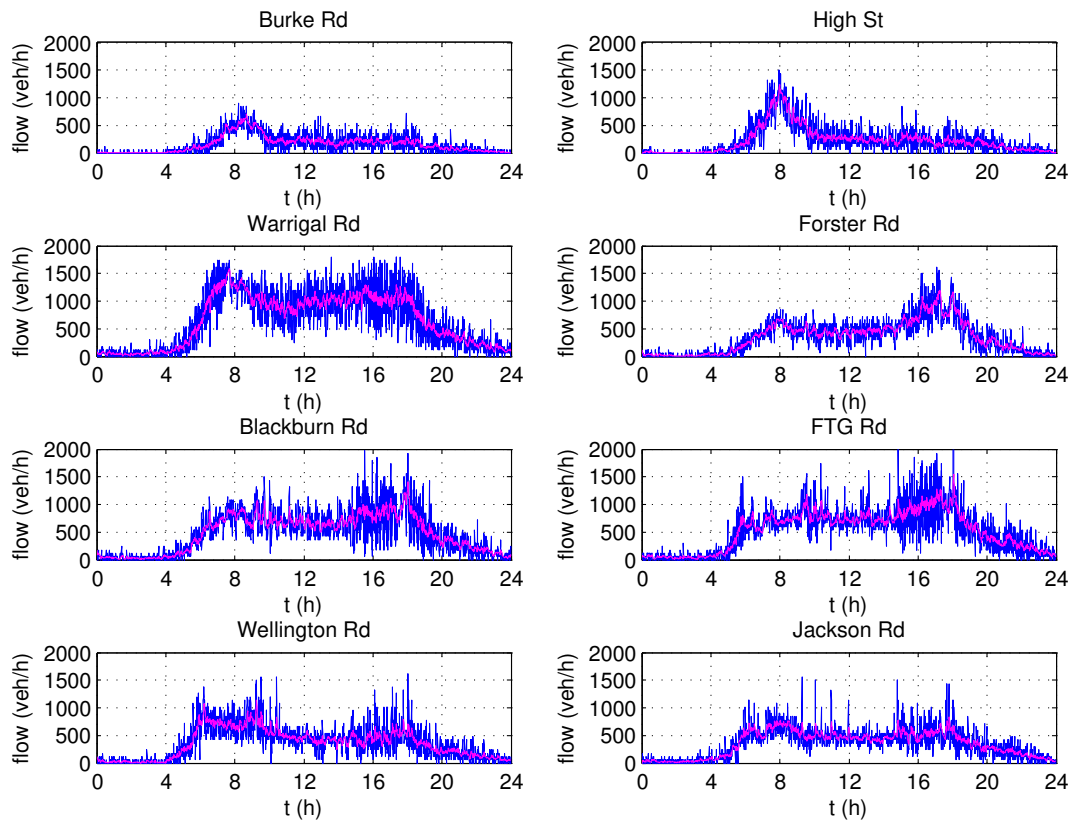smoothed (red line) flow at the off-ramps, Monday 15-08-2016

FIGURE A.4: Comparison between measured (blue line) and smoothed (red line) flow at the on-ramps, Monday 15-08-2016
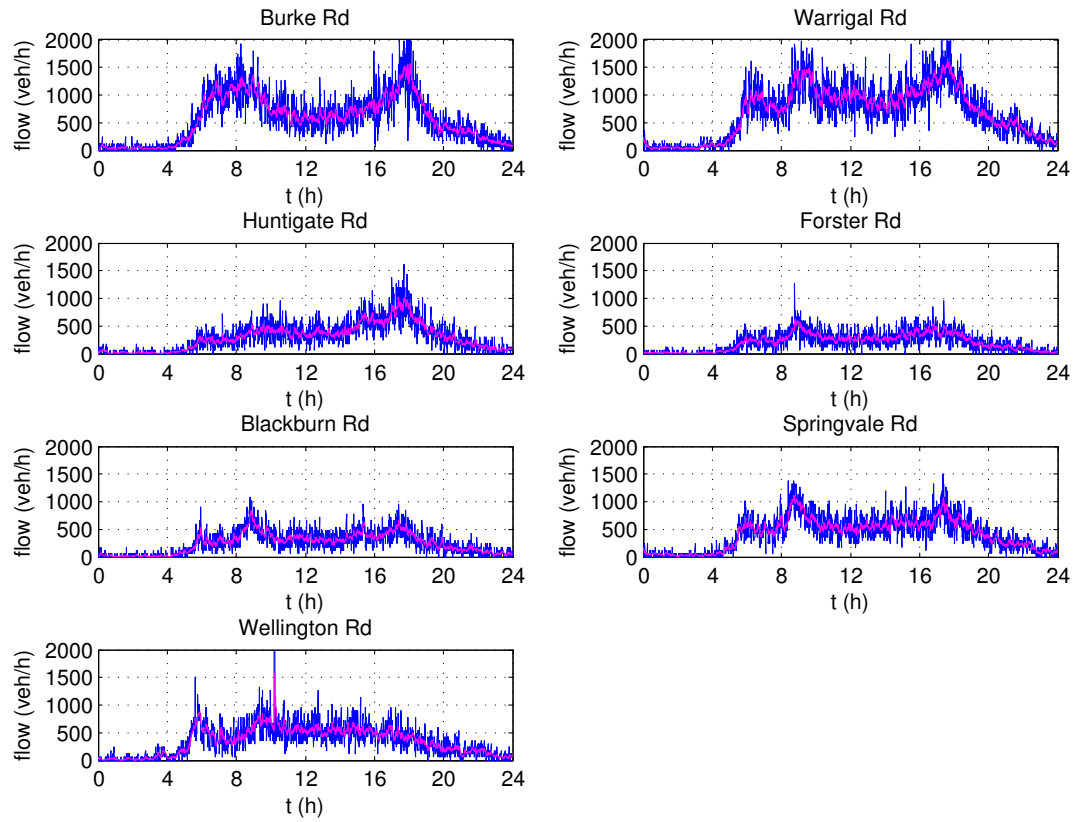
FIGURE A.5:   Comparison between measured (blue line) and smoothed (red line) flow at the off-ramps, Tuesday 16-08-2016
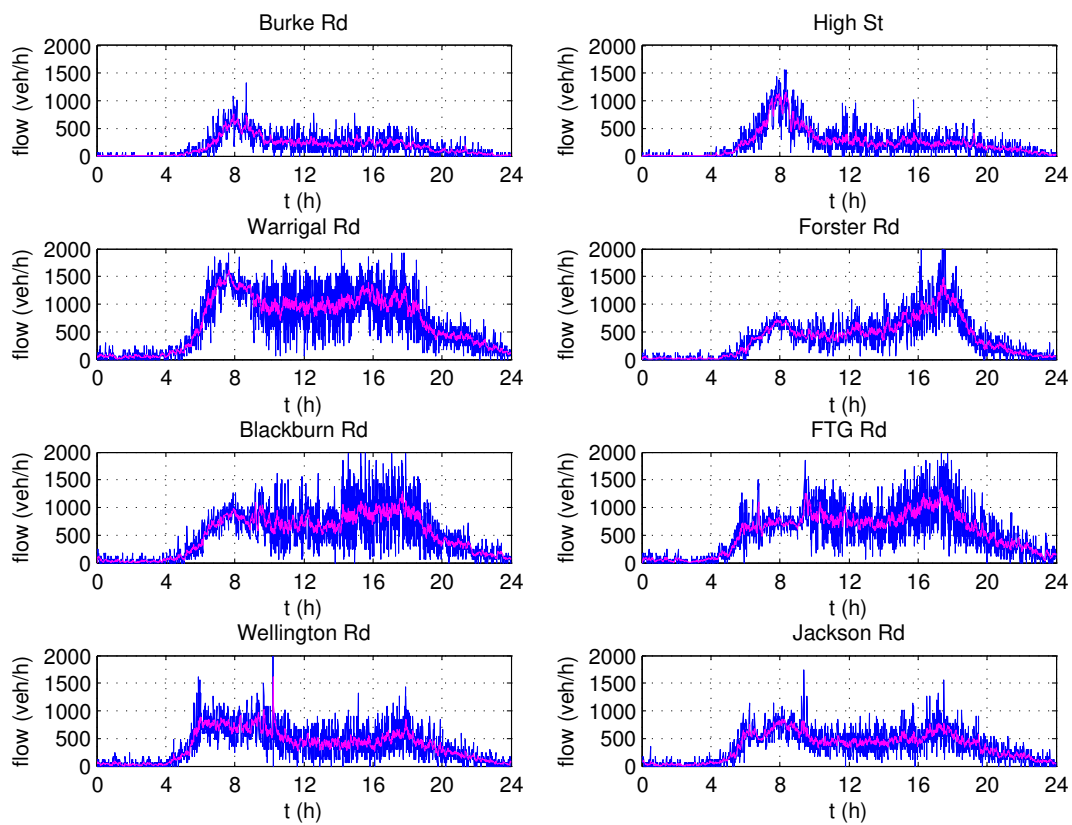
FIGURE A.6: Comparison between measured (blue line) and smoothed (red line) flow at the on-ramps, Tuesday 16-08-2016

# Appendix B

# Appendix B

In this Appendix the graphs of variable speed limits for each detector are presented for the days used for calibration and validation.

- Figure B.1 illustrates the displayed VSLs for Friday 11-11-2016. The displayed speed for the first two VMSs gantries is 100 km/h for the first thirty minutes and for the rest of the examined period it is 80 km/h. The following three VMSs gantries, as well as the last one set the displayed speed equal to the nominal speed. Finally, the rest five gantries temporarily, at about 08:15 AM, set the displayed speed to 60 km/h, while for the rest of the examined period the VSLs are equal to the nominal speed limit.

- Figure B.2 illustrates the displayed VSLs for Monday 15-08-2016. The graphs are quite clear for this day. Almost all the VSMs gantries set the VSLs equal to 100 km/h, except from the first two VMSs gantries in which temporarily at the beginning of the examined period the displayed speed is 80 km/h.

- Figure B.3 illustrates the displayed VSLs for Tuesday 16-08-2016 05:00-11:00 AM. As it is presented the displayed speed from VMSs gantries is equal to the nominal speed limit for the whole time window considered in this study, except the first two VMSs gantries, where the displayed speed is 80 km/h.
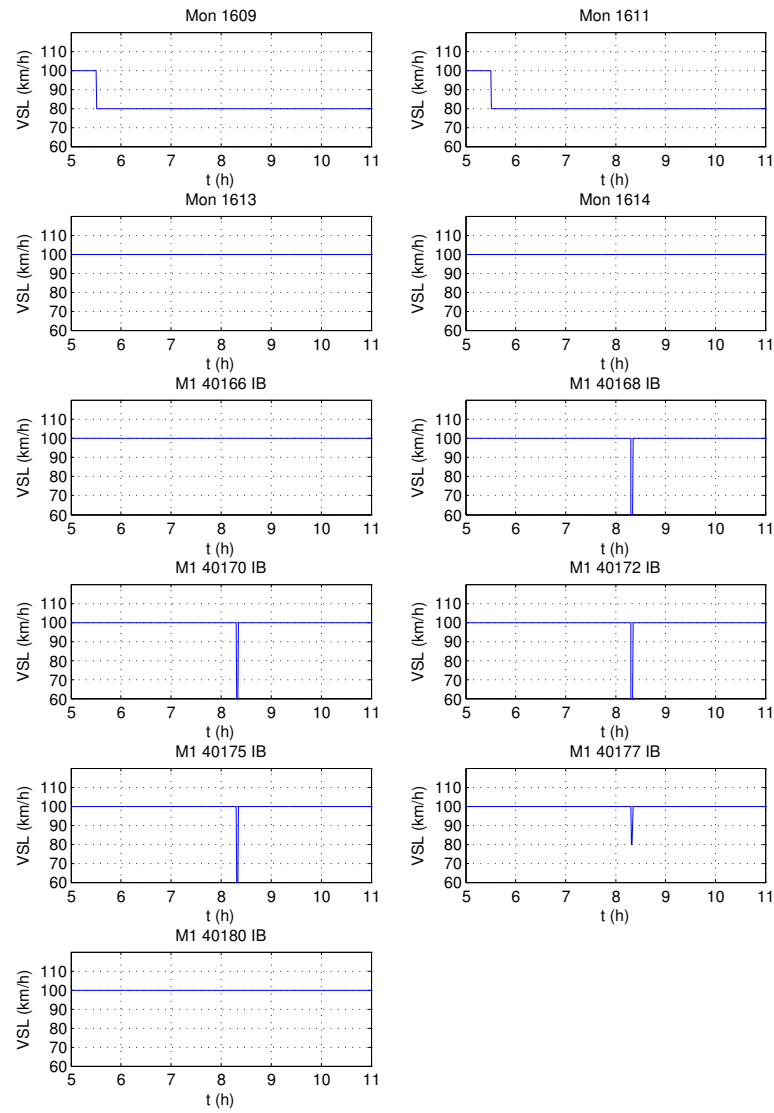
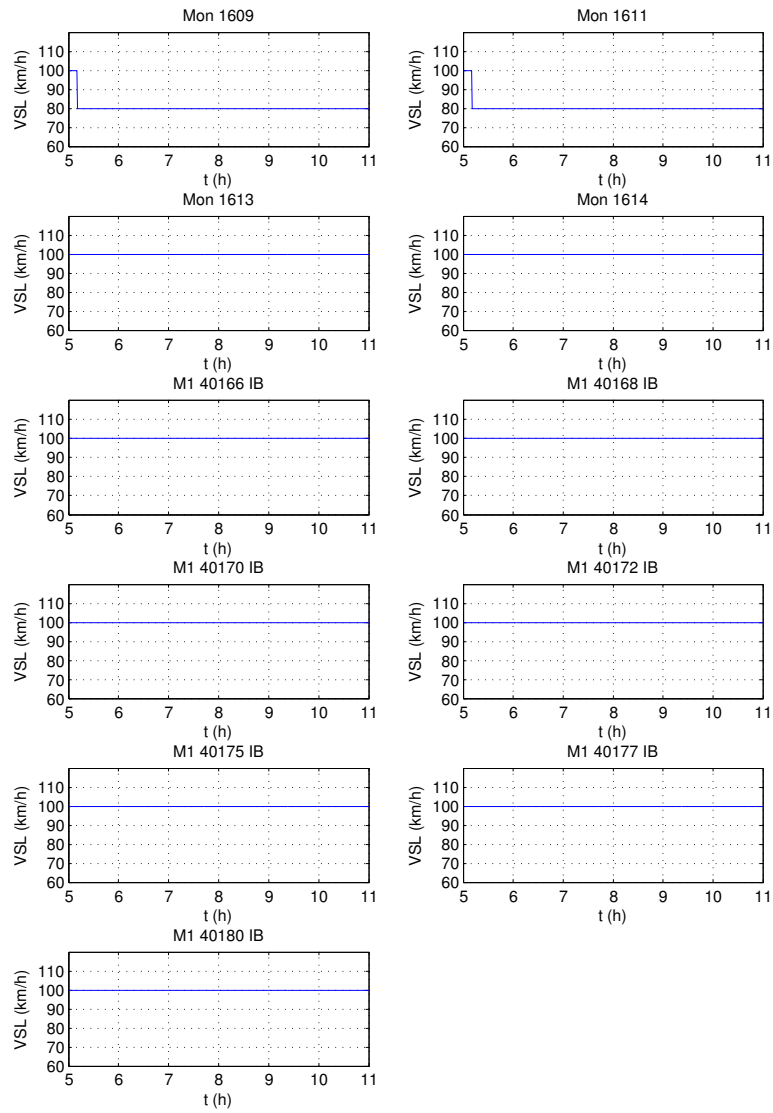FIGURE B.1: Variable Speed Limits for Friday 11-11-2016 05:00-11:00
AM

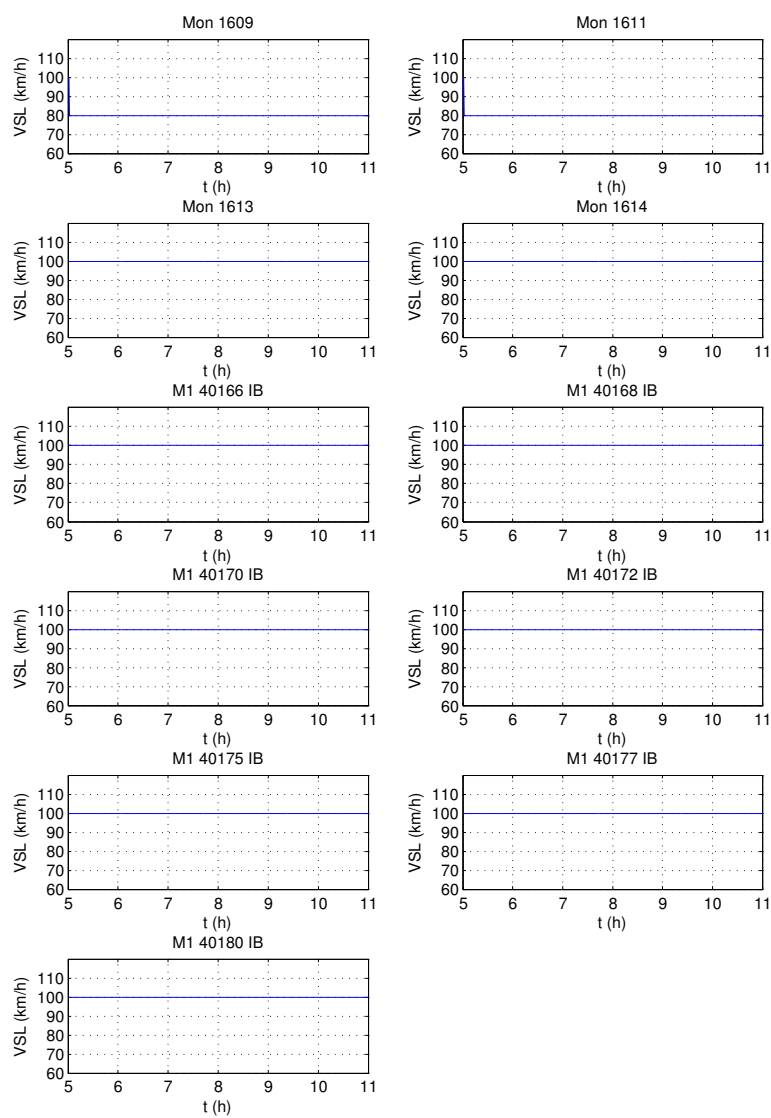FIGURE B.2: Variable Speed Limits for Monday 15-08-2016 05:00-11:00 AM

FIGURE B.3:  Variable Speed Limits for Tuesday 16-08-2016 05:00-
11:00 AM

# Bibliography

[1] M. Papageorgiou and A. Kotsialos, "Freeway ramp metering: An overview", in *Intelligent Transportation Systems*, IEEE, 2000, pp. 228–239.

[2] D. Schrank, B. Eisele, and T. Lomax, "TTI's 2012 urban mobility report", *Texas A&M Transportation Institute. The Texas A&M University System*, p. 4, 2012.

[3] H. M. Zhang and S. G. Ritchie, "Freeway ramp metering using artificial neural networks", *Transportation Research Part C: Emerging Technologies*, vol. 5, no. 5, pp. 273–286, 1997.

[4] M. Papageorgiou, E. Kosmatopoulos, and I. Papamichail, "Effects of variable speed limits on motorway traffic flow", *Transportation Research Record: Journal of the Transportation Research Board*, no. 2047, pp. 37–48, 2008.

[5] S. Cohen, M. Ayot, and N. Duc, "Guide méthodologique: Enjeux des mesures de régulation dynamique de vitesses", *INRETS and LEE*, p. 121, 2008.

[6] S. P. Hoogendoorn and P. H. Bovy, "State-of-the-art of vehicular traffic flow modelling", *Proceedings of the Institution of Mechanical Engineers, Part I: Journal of Systems and Control Engineering*, vol. 215, no. 4, pp. 283–303, 2001.

[7] A. Messner and M. Papageorgiou, "METANET: A macroscopic simulation program for motorway networks", *Traffic engineering & control*, vol. 31, no. 8-9, pp. 466–470, 1990.

[8] A. Spiliopoulou, M. Kontorinaki, M. Papageorgiou, and P. Kopelias, "Macroscopic traffic flow model validation at congested freeway off-ramp areas", *Transportation Research Part C: Emerging Technologies*, vol. 41, pp. 18–29, 2014.

[9] S. Singer and J. Nelder, "Nelder-mead algorithm", *Scholarpedia*, vol. 4, no. 7, p. 2928, 2009.

[10] L. I. Panis, S. Broekx, and R. Liu, "Modelling instantaneous traffic emission and the influence of traffic speed limits", *Science of the total environment*, vol. 371, no. 1, pp. 270–285, 2006.

[11] S. K. Zegeye, B. De Schutter, H. Hellendoorn, and E. Breunesse, "Model-based traffic control for balanced reduction of fuel consumption, emissions, and travel time", *IFAC Proceedings Volumes*, vol. 42, no. 15, pp. 149–154, 2009.

[12] S. Zegeye, B. De Schutter, J. Hellendoorn, and E. Breunesse, "Variable speed limits for area-wide reduction of emissions", in *Intelligent Transportation Systems (ITSC), 2010 13th International IEEE Conference on*, IEEE, 2010, pp. 507–512.

[13] H. Zackor, "Beurteilung verkehrsabhängiger geschwindigkeitsbeschränkungen auf autobahnen", *STRASSENBAU U STRASSENVERKEHRSTECH*, no. 128, 1972.

[14] H. Zackor and M. Papageorgiou, "Speed limitation on freeways: Traffic-responsive strategies", *Concise encyclopedia of traffic and transportation systems*, pp. 507–511, 1991.

[15] A. Hegyi, "Model predictive control for integrating traffic control measures", PhD thesis, Delft University of Technology, The Netherlands, 2004.

[16] I. Papamichail, K. Kampitaki, M. Papageorgiou, and A. Messmer, "Integrated ramp metering and variable speed limit control of motorway traffic flow", *IFAC Proceedings Volumes*, vol. 41, no. 2, pp. 14 084–14 089, 2008.

[17] H. J. Payne, "Models of freeway traffic and control.", *Mathematical models of public systems*, 1971.

[18] M. Papageorgiou, J.-M. Blosseville, and H. Hadj-Salem, "Modelling and real-time control of traffic flow on the southern part of boulevard peripherique in paris: Part i: Modelling", *Transportation Research Part A: General*, vol. 24, no. 5, pp. 345–359, 1990.

[19] K. Kampitaki, "Integrated control of traffic flow using ramp metering and variable speed limits", MSc Thesis, Dept. Prod. Eng. Manage., Tech. Univ. Crete, Chania, Greece, 2008.

[20] D. Ngoduy and M. J. Maher, "Calibration of second order traffic models using continuous cross entropy method", *Transportation Research Part C: Emerging Technologies*, vol. 24, pp. 102–121, 2012.

[21] C. F. Daganzo, "The cell transmission model, part ii: Network traffic", *Transportation Research Part B: Methodological*, vol. 29, no. 2, pp. 79–93, 1995.

[22] J. C. Lagarias, J. A. Reeds, M. H. Wright, and P. E. Wright, "Convergence properties of the nelder–mead simplex method in low dimensions", *SIAM Journal on optimization*, vol. 9, no. 1, pp. 112–147, 1998.

[23] A. Spiliopoulou, I. Papamichail, M. Papageorgiou, Y. Tyrinopoulos, and J. Chrysoulakis, "Macroscopic traffic flow model calibration using different optimization algorithms", *Operational Research*, vol. 17, no. 1, pp. 145–164, 2017.

[24] A. Kotsialos, M. Papageorgiou, C. Diakaki, Y. Pavlis, and F. Middelham, "Traffic flow modeling of large-scale motorway networks using the macroscopic modeling tool metanet", *IEEE Transactions on intelligent transportation systems*, vol. 3, no. 4, pp. 282–292, 2002.